T CELLS

Emergence and fate of stem cell–like *Tcf7*$^+$ CD8$^+$ T cells during a primary immune response to viral infection

Joana Gomes Silva[1]†, Daniela Pais Ferreira[1]†‡, Alexandre Dumez[1]†, Tania Wyss[2], Romain Veber[1], Maxime Danilo[1]§, Daniel D. Pinschewer[3], Mélanie Charmoy[1], Werner Held[1]*

In response to infection, naïve CD8$^+$ T (T_N) cells yield a large pool of short-lived terminal effector (T_{TE}) cells that eliminate infected host cells. In parallel, a minor population of stem cell–like central memory (T_{CM}) cells forms, which has the capacity to maintain immunity after pathogen clearance. It has remained uncertain whether stem-like T_{CM} cells arise by dedifferentiation from a subset of cytolytic T_{TE} cells or whether priming generates stem-like cells capable of seeding the T_{CM} compartment and, if so, when cytolytic T_{TE} cells branch off. Here, we show that CD8$^+$ T cells with stem-like properties, which are identified by the expression of TCF1 (encoded by *Tcf7*), are present across the primary response to infection. Priming programs T_N cells to undergo multiple cell divisions, over the course of which TCF1 expression is maintained. These TCF1$^+$ cells further expand relatively independently of systemic inflammation, antigen dose, or affinity, and they quantitatively yield TCF1$^+$ T_{CM} cells after pathogen clearance. Inflammatory signals suppress TCF1 expression in early divided TCF1$^+$ cells. TCF1 down-regulation is associated with the irreversible loss of self-renewal capacity and the silencing of stem/memory genes, which precedes the stable acquisition of a T_{TE} state. TCF1 expression restrains cell cycling, explaining in part the limited expansion of TCF1$^+$ relative to TCF1$^-$ cells during the primary response. Thus, our data are consistent with terminal differentiation of effector cells being a step-wise process that is initiated by inflammation in primed stem-like cells, which would otherwise become central memory cells by default.

INTRODUCTION

Infection activates very rare naïve antigen-specific CD8$^+$ T (T_N) cells, which expand and differentiate into cytolytic effector cells that are needed to clear pathogen-infected cells. Although most of the effector CD8$^+$ T cells are terminally differentiated and die after pathogen clearance [referred to as terminal effector (T_{TE}) cells], 5 to 10% of the responding cells persist after pathogen clearance and form a diverse memory CD8$^+$ T cell compartment. The latter includes central memory T (T_{CM}) cells, which maintain immunity to subsequent infections with the same pathogen thanks to their stem cell–like potential to expand, differentiate into effector cells, or self-renew (*1*). Several models have been proposed to explain the relationship between the distinct CD8$^+$ T cell states, the predominance of effector cells during the acute phase of the immune response, and the emergence of memory cells after antigen clearance (*2*–*5*). The linear differentiation model suggests that T_N cells expand and acquire cytotoxic capacity. Once infection is cleared, occasional cells dedifferentiate to become noncytolytic T_{CM} cells (*6*, *7*). Dedifferentiation is not random, because one subpopulation of effector stage CD8$^+$ T cells, termed memory precursor effector cells (MPECs), are biased toward memory fate (*8*–*10*), although they do not quantitatively yield memory. Irrespectively, MPECs express granzyme B (GzmB), have cytotoxic activity (*8*), and would, thus, need to dedifferentiate to yield noncytolytic T_{CM} cells. In support of this model, the *Sell* locus (encoding CD62L) has inhibitory DNA methylation marks in MPEC but is demethylated in T_{CM} cells (*7*). Alternative scenarios include the so-called progressive differentiation model, which proposes that short-lived effector cells derive from precursors of long-lived cells (*2*–*5*, *11*–*14*). Epigenetic repression of memory associated genes is needed for efficient effector differentiation (*15*–*17*). Here, the level of antigenic, costimulatory, and inflammatory signals that individual cells accumulate is thought to determine the proliferation and differentiation of these precursors. According to this model, stem-like cells would be required to be present throughout the primary response to infection; however, that had not been formally demonstrated.

The developmental relationship between T_{CM} and T_{TE} cells may be followed using the expression of the transcription factor TCF1 (T cell factor 1) (encoded by the *Tcf7* gene), which is required for the generation of T_{CM} cells but dispensable for T_{TE} formation (*18*–*20*). T_N cells express high levels of TCF1, and most CD8$^+$ T cells lose expression after day 3 of lymphocytic choriomeningitis virus (LCMV) infection, and this is associated with effector differentiation. However, a small population of *Tcf7*$^+$ cells is detected throughout the primary response to infection (*21*, *22*). In addition, effector stage cells expressing the central memory marker CD62L have been observed in bacterial (*Listeria monocytogenes*) (*23*–*25*) and LCMV infection (*26*) where they overlap in part with *Tcf7*$^+$ cells (*22*). *Tcf7*$^+$ cells present during the expansion phase [day 5 (d5) after LCMV infection] have the potential to yield T_{CM} cells after transfer into infection time-matched secondary hosts. On the other hand, d5 *Tcf7*$^-$ cells fail to yield T_{CM} cells and remain *Tcf7*$^-$ (*21*). Lineage tracing subsequently revealed that the *Tcf7*$^+$ cells present at the peak of the response (d8) quantitatively and exclusively yield T_{CM} cells (*22*), in line with the inferred trajectory of these cells based on single-cell RNA sequencing (scRNA-seq) analysis (*27*). The d8

[1]Department of Oncology, University of Lausanne, Lausanne, Switzerland. [2]Translational Data Science Facility, Swiss Institute of Bioinformatics, Lausanne, Switzerland. [3]Department of Biomedicine, Division of Experimental Virology, University of Basel, Basel, Switzerland.
*Corresponding author. Email: werner.held@unil.ch
†These authors contributed equally to this work.
‡Present address: Ichnos Sciences Biotherapeutics SA, Epalinges, Switzerland.
§Present address: Department of Oncology, Centre Hospitalier Universitaire Vaudois, Lausanne, Switzerland.

Tcf7$^+$ cells thus qualify as central memory precursors (T_{pCM}). T_{pCM} cells closely resemble T_{CM} cells as judged by their comparable phenotype, lack of cytolytic activity, and stem cell–like potential in recall stimulation experiments, whereby TCF1 is essential for the self-renewal of T_{pCM} cells (*22*). The presence of stem-like *Tcf7*$^+$ CD8$^+$ T cells at the peak of the response indicated that *Tcf7*$^+$ cells might display stem cell–like potential and central memory precursor function throughout the primary response to infection. If so, it was unknown when and under what conditions these *Tcf7*$^+$ cells committed toward differentiation and how this translated into changes in stemness and effector programs.

Here, we show that TCF1$^+$ CD8$^+$ T cells maintain stem cell–like potential and central memory precursor function throughout the primary immune response, but that only the TCF1$^+$ cells present during priming can yield TCF1$^-$ T_{TE} cells. Priming programs cells to undergo multiple cell divisions while retaining TCF1. The presence of type I interferon (IFN-I) during cell division, rather than the priming phase, down-regulates TCF1, resulting in the stable loss of stemness. Thus, dividing TCF1$^+$ cells that are committed to become T_{CM} cells can be deviated toward T_{TE} differentiation by inflammatory cytokine–induced TCF1 suppression.

RESULTS

Tcf7$^+$ CD8$^+$ T cells are present throughout the primary immune response to infection

We have recently shown that *Tcf7*$^+$ CD8$^+$ T cells present at the peak of the primary response to LCMV infection display key features of T_{CM} cells (*22*). Here, we used scRNA-seq to address whether transcriptionally similar cells were present throughout the primary CD8$^+$ T cell response to infection. We adoptively transferred naïve P14 CD8$^+$ T cells (CD45.2), which express a transgenic T cell receptor (TCR) specific for the LCMV gp33-41 epitope presented by H-2D^b, into C57BL/6 (B6) recipients (CD45.1 or CD45.1/2). Mice were then infected with LCMV strains, which cause acute resolving infection. On d0 (naïve), d2, d3, d4, and d6 postinfection (p.i.), splenic P14 cells were identified (fig. S1, A and B), flow-sorted, and subjected to scRNA-seq analysis, obtaining 19,374 high-quality cells for further analysis (data file S1).

Compared with T_N cells (d0), the average number of unique molecular identifiers and genes was transiently increased in d2 and d3 cells (fig. S1C). On the basis of uniform manifold approximation and projection (UMAP) dimensionality reduction, T_N (d0), d2, and d6 cells were portioned into discrete areas, whereas d3 and d4 cells partially comingled, indicating substantial transcriptome changes (Fig. 1A). We addressed whether cells that were transcriptomically similar to T_{pCM} cells were present throughout the primary immune response. To this end, we calculated a T_{pCM} gene signature score (data file S2) (*22*). Whereas almost all T_N and d2 cells had a positive T_{pCM} score, the presence of such cells was reduced on d3, d4, and d6 p.i. Notwithstanding, T_{pCM} score-positive and *Tcf7*$^+$ cells were detected at each time point (Fig. 1, B to D). Very similar results were obtained using a T_{CM} gene signature score (fig. S1D and data file S2) (*22*).

To track and eventually isolate TCF1-expressing P14 cells during the primary immune response, we used a *Tcf7*^{GFP} reporter mouse strain (*28*). *Tcf7*^{GFP} was highly expressed in virtually all T_N and most d2 cells but was down-regulated in most cells from d4 p.i. However, 2 to 10% of cells retained *Tcf7*^{GFP} expression in response to a low dose [2×10^5 plaque-forming units (PFU)] of LCMV Armstrong (Arm) strain (Fig. 1E), a 10-fold higher LCMV Arm dose (fig. S1, E and F), or LCMV WE (*22*), a LCMV strain with broader tissue tropism compared with Arm (*29*). The *Tcf7*$^{GFP+}$ cells expanded between d4 and d6 p.i., although at a reduced rate compared with *Tcf7*$^{GFP-}$ cells (Fig. 1F). A considerable fraction of the *Tcf7*$^{GFP+}$ cells expressed CD62L, CD127, IFN-γ, and interleukin-2 (IL-2) at all time points, whereas a subset of these cells expressed GzmB (but not GzmA) at d2 and d4 but not at later stages of the primary response (fig. S2) as shown before (*22*). Thus, CD8$^+$ T cells with phenotypic and transcriptional similarity to T_{pCM} and T_{CM} cells were present throughout the primary response to acute infection.

The stem-like potential of *Tcf7*$^+$ CD8$^+$ T cells is retained throughout the primary immune response

Tcf7 is expressed by CD8$^+$ T cells with stem cell–like potential. Therefore, we investigated whether the early *Tcf7*$^{GFP+}$ cells had the capacity to expand and self-renew or differentiate in response to recall stimulation. We isolated *Tcf7*$^{GFP+}$ and *Tcf7*$^{GFP-}$ P14 cells from the various time points of infection and retransferred them into naïve secondary recipients that were then infected with LCMV. Eight days later (dx+8), *Tcf7*$^{GFP+}$ cells had expanded about 10^4-fold, irrespective of the time point of isolation from primary hosts, very similar to that of T_N (d0+8) or T_{CM} cells (d28+8) (Fig. 1G). *Tcf7*$^{GFP+}$ cells yielded more progeny than *Tcf7*$^{GFP-}$ cells isolated from the same time point (Fig. 1G). Primary *Tcf7*$^{GFP-}$ cells produced only *Tcf7*$^{GFP-}$ offspring, most of which had a T_{TE} phenotype (Klrg1$^+$ CD127$^-$ CD62L$^-$) (Fig. 1H and fig. S3). Primary *Tcf7*$^{GFP+}$ cells yielded more diverse progeny, including *Tcf7*$^{GFP-}$ Klrg1$^+$, *Tcf7*$^{GFP-}$ Klrg1$^-$, and secondary *Tcf7*$^{GFP+}$ cells (Fig. 1H and fig. S3). The latter lacked Klrg1 but frequently expressed CD127 and occasionally CD62L (fig. S3). Secondary *Tcf7*$^{GFP+}$ cells derived comparably from T_N and d2 *Tcf7*$^{GFP+}$ cells but were generated less efficiently from later *Tcf7*$^{GFP+}$ cells, although the output was still equivalent or superior in number to that from T_{CM} cells (d28+8) (Fig. 1H). The regeneration capacity of *Tcf7*$^{GFP+}$ cells thus declined with the progression of the primary response (Fig. 1H). This decline was not related to a change in the fraction of *Tcf7*$^+$ cells coexpressing CD62L (fig. S2A). Moreover, the d8 *Tcf7*$^+$ CD62L$^+$ and *Tcf7*$^+$ CD62L$^-$ subsets had comparable recall expansion and regeneration capacity, as judged by the generation of secondary *Tcf7*$^{GFP+}$ cells (fig. S4). Thus, the presence of *Tcf7*$^+$ cells lacking CD62L at d8 p.i. did not explain the reduced stemness compared with d0 cells. We conclude that *Tcf7*$^+$ CD8$^+$ T cells retain stem-like potential throughout the immune response but that their regeneration capacity declines. The latter may be related to the number of prior cell divisions, as recently suggested for T_{CM} cells (*30*).

Tcf7$^+$ CD8$^+$ T cells maintain the capacity to become T_{CM}, but their ability to form differentiated subsets declines with time after infection

Because *Tcf7*$^+$ CD8$^+$ T cells had stem cell–like potential as judged by the response to recall stimulation, we next addressed their capacity to yield short-lived effector cells (T_{TE}) or memory cell subsets [T_{CM}; effector memory (T_{EM}) or tissue-resident memory (T_{RM})] during the immune response. We used a *Tcf7*-guided fate mapping approach based on a *Tcf7*$^{GFP\text{-}CreERT2}$ mouse strain (*Tcf7*$^{GFP\text{-}iCre}$) (*22*) combined with a Rosa26^{TdTomato} (*R26*^{Tom}) reporter allele to

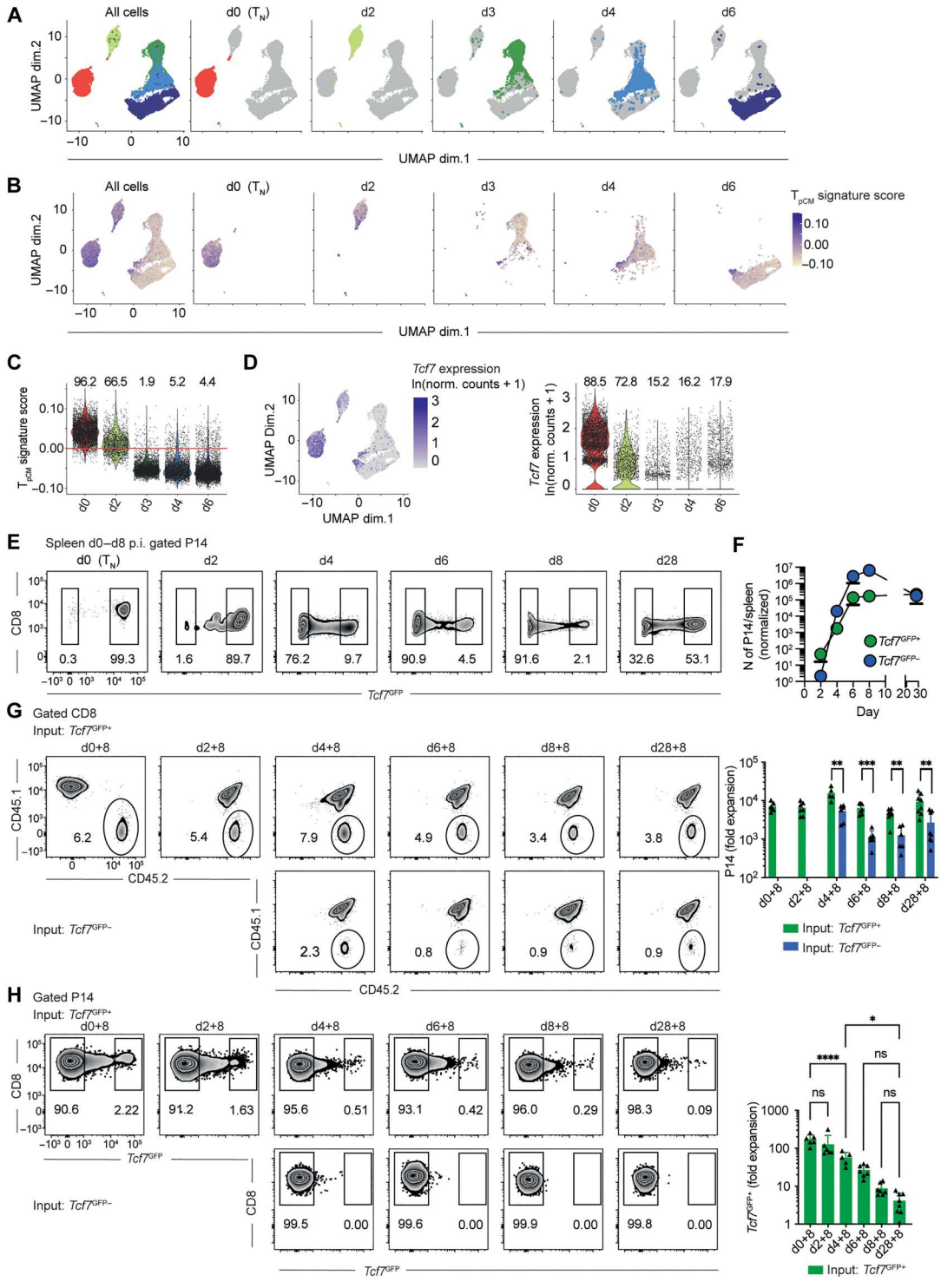

Fig. 1. Presence and stemness of *Tcf7*$^{+}$ CD8^{+} T cells during the primary response to infection. (A to D) B6 mice (CD45.1) were adoptively transferred with naïve *Tcf7*^{GFP} P14 cells (CD45.2) and infected with LCMV Arm. P14 cells (CD45.2) were flow-sorted on d0 (naïve, T_N), d2, d3, d4, and d6 p.i. and subjected to scRNA-seq analysis. (**A**) UMAP dimensionality reduction of P14 cells analyzed at d0 (T_N) (n = 5123), d2 (n = 1572), d3 (n = 3974), d4 (n = 3352), and d6 (n = 5353) p.i. (**B**) UMAP plot of individual P14 cells colored according to their level of expression of a T_{pCM} signature score [genes up-regulated in d8 *Tcf7*$^{+}$ (T_{pCM}) versus d8 *Tcf7*$^{-}$ cells]. (**C**) Distribution of the T_{pCM} score at the indicated time points of the primary response. The percentage of cells with a T_{pCM} score greater than 0 is shown above each time point. (**D**) UMAP and violin plots showing the distribution of the expression of *Tcf7* [ln(norm. counts + 1)] in individual P14 cells and the presence of *Tcf7*$^{+}$ cells at distinct time points of the primary response. (**E** to **H**) B6 mice (CD45.1/2) were adoptively transferred with *Tcf7*^{GFP} P14 cells (CD45.2) and infected with LCMV Arm. (E) Splenic P14 cells were analyzed for *Tcf7*^{GFP} expression at the indicated time points p.i. (F) Number (N) of *Tcf7*$^{GFP+}$ (green) and *Tcf7*$^{GFP-}$ P14 cells (blue) per spleen, normalized to an input of 10^4 cells. (G and H) *Tcf7*$^{GFP+}$ and *Tcf7*$^{GFP-}$ P14 cells (CD45.2) were flow-sorted at the indicated time points p.i. and transferred into naïve WT mice (CD45.1 or CD45.1/2) that were infected with LCMV Arm. (G) Recipient mice were analyzed 8 days later (dx+8). The bar graph shows the fold expansion of P14 cells compared with input (assuming 10% take). (H) Recipient mice were analyzed for the presence of secondary *Tcf7*$^{GFP+}$ P14 cells (green), and the bar graph depicts the fold expansion compared with input (assuming 10% take). Data shown in (E) to (H) are compiled from two experiments with a total of six to nine mice per time point or group. Data points in (F) to (H) represent individual mice. Bar graphs show means (±SD). Statistics in (G) are based on multiple unpaired two-tailed Student's t test and in (H) on two-way ANOVA with Fisher least significant difference (LSD) test, whereby ****P < 0.0001; ***P < 0.001; **P < 0.01; *P < 0.05; and ns, P > 0.05.

determine the fate of the stem-like CD8$^+$ T cells during a primary immune response without adoptive cell transfers. A single dose of tamoxifen (TAM) induced Tom expression in a sizeable fraction of *Tcf7*$^+$ cells, whereby the effective TAM half-life was around 12 hours (fig. S5).

In our previous work, when fate mapping was initiated on d8 after LCMV infection, we found that virus-specific d8 *Tcf7*$^+$ cells yielded *Tcf7*$^+$ T_{CM} but essentially no *Tcf7*$^-$ T_{EM} or short-lived T_{TE} cells (*22*). To determine whether *Tcf7*$^+$ CD8$^+$ T cells yielded T_{CM} or differentiated *Tcf7*$^-$ progeny at earlier time points of infection, we initiated fate mapping on d1, d2, d3, or d4 p.i. (Fig. 2A). Tom-labeled CD8$^+$ T cells, which retained *Tcf7*^{GFP} expression (Tom$^+$ *Tcf7*$^{GFP\text{-}iCre+}$), were observed both on d8 and d28 p.i., irrespective of when labeling was started (Fig. 2, B and E). Some of these Tom$^+$ *Tcf7*$^{GFP\text{-}iCre+}$ cells expressed CD62L, and most lacked Klrg1 both at d8 and d28 p.i. (Fig. 2, C and F), consistent with a T_{pCM}/T_{CM} phenotype. The abundance of Tom$^+$ *Tcf7*$^{GFP\text{-}iCre+}$ cells at d8 and at d28 p.i. was comparable (Fig. 2H), indicating that *Tcf7*$^+$ CD8$^+$ T cells quantitatively generated T_{CM} cells. Similar data were obtained when fate mapping was performed using a Rosa26$^{lox\ stop\ lox\ Confetti}$ (*R26*^{Confetti}) reporter allele (fig. S6). Fate mapping thus showed that *Tcf7*$^+$ cells present throughout the primary response gave rise to T_{CM} cells and thus qualified as T_{pCM} cells.

In addition, fate-mapping of *Tcf7*$^+$ cells at d1, d2, d3, or d4 yielded Tom$^+$ memory cells (d28 p.i.) that no longer expressed *Tcf7* (Tom$^+$ *Tcf7*$^{GFP\text{-}iCre-}$) (Fig. 2, E and I). These cells lacked CD62L, but many expressed Klrg1 (Fig. 2G), consistent with a T_{EM} phenotype. The ability of *Tcf7*$^+$ cells to yield *Tcf7*$^-$ memory cells declined as the primary response progressed (Fig. 2I), and we have previously shown that this no longer occurred from d8 *Tcf7*$^+$ cells (*22*).

Tom$^+$ *Tcf7*$^{GFP\text{-}iCre-}$ cells were also observed at the peak of the primary response (d8 p.i.) (Fig. 2, B and J). These cells lacked CD62L, but most of them expressed Klrg1 (Fig. 2D). When labeling of *Tcf7*$^+$ cells was started at d1 or d2, Tom$^+$ *Tcf7*$^{GFP\text{-}iCre-}$ cells were more abundant at d8 than at d28 (Fig. 2J), consistent with d1 and d2 *Tcf7*$^+$ cells generating short-lived T_{TE} cells that disappeared after viral clearance. In contrast, the abundance of Tom$^+$ *Tcf7*$^{GFP\text{-}iCre-}$ cells at d8 and d28 was not different when labeling was started at d3 or d4 (Fig. 2J), indicating that T_{TE} cells were no longer generated. Corresponding data were obtained when lineage tracing was performed using a *R26*^{Confetti} reporter allele (fig. S6). Moreover, fate mapping of antigen-specific *Tcf7*$^+$ cells, recognizing the gp33 and the np396 epitopes, from a polyclonal population confirmed that d4 *Tcf7*$^+$ cells yielded *Tcf7*$^+$ and *Tcf7*$^-$ memory cells but not short-lived T_{TE} cells (fig. S7, A to F). In addition, d2 *Tcf7*$^+$ cells were the main source of T_{RM} cells present among intestinal intraepithelial lymphocytes (IELs) at d28 p.i. (fig. S7, G to I).

To confirm that *Tcf7*$^+$ cells did not yield T_{TE} cells after d2 p.i., we delayed the adoptive transfer of naïve P14 cells relative to the time of infection (Fig. 3A). Compared with the transfer of naïve P14 cells at the time of infection (d0), P14 transfer at d3 p.i. resulted in a 41.9-fold reduced expansion of P14 cells at d8 p.i. (Fig. 3B). The formation of *Tcf7*$^{GFP-}$ Klrg1$^+$ P14 cells was reduced 107-fold, whereas that of *Tcf7*$^{GFP+}$ P14 cells was only reduced 5.5-fold (Fig. 3C). The latter cells expressed CD62L and produced IL-2 (fig. S8), similar to T_{pCM} cells.

Thus, our data are consistent with *Tcf7*$^+$ cells having stemness and maintaining the ability to form T_{CM} cells, but they are unable to become T_{TE} and T_{RM} cells efficiently after d2 and cease to yield T_{EM} cells between d4 and d8 p.i. Moreover, our data indicate that the antigenic/inflammatory environment at d3 p.i. generated *Tcf7*$^+$ cells relatively efficiently but no longer resulted in T_{TE} formation.

Tcf7$^+$ CD8$^+$ T cells no longer contribute to the pool of short-lived effectors 4 days p.i. but seed memory subsets

Despite the presence of *Tcf7*$^+$ CD8$^+$ T cells throughout the immune response, fate mapping suggested that these cells no longer contributed to the T_{TE} pool after d4 p.i. To independently address this, we used T cells from *Tcf7*$^{DTR\text{-}GFP}$ transgenic mice (*31*), whereby the expression of the diphtheria toxin receptor (DTR) allowed *Tcf7*-expressing cells to be selectively ablated in vivo. We transferred *Tcf7*$^{DTR\text{-}GFP}$ (or control *Tcf7*^{GFP}) P14 cells to B6 mice and treated with diphtheria toxin (DT) at d4 and d5 after LCMV Arm infection (Fig. 3D). At d6 p.i., the spleens of mice transferred with *Tcf7*$^{DTR\text{-}GFP}$ P14 cells harbored 48-fold fewer *Tcf7*$^+$ P14 cells than control mice, whereas the number of *Tcf7*$^-$ P14 cells was not different (about 10^6 cells) (Fig. 3E), demonstrating that DT treatment ablated selectively *Tcf7*$^+$ cells. Independent of the ablation of *Tcf7*$^+$ P14 cells, *Tcf7*$^-$ P14 cells had expanded to about 10^7 cells at d8 (Fig. 3F), and both had contracted at d16 p.i. (Fig. 3, F and G), indicating that the short-lived effector T_{TE} cell pool indeed derived from *Tcf7*$^-$ rather than *Tcf7*$^+$ cells present on d4 of the infection.

We evaluated the memory compartment at 16 p.i., because the mice lose weight about 10 days after DT injection (d14 p.i.) independently of the presence of DT-sensitive cells (*32*). We found that the deletion of d4 *Tcf7*$^+$ cells reduced the presence of *Tcf7*$^-$ cells (T_{EM}) (4.6-fold) (Fig. 3G) and that of CD62L$^+$ Klrg1$^-$ (52-fold) and IL-2$^+$ cells (6-fold) (T_{CM}) (Fig. 3, H and I), indicating that the formation of T_{EM} and T_{CM} did depend on d4 *Tcf7*$^+$ cells. In contrast, as previously found, d10 *Tcf7*$^+$ cells did not yield T_{EM} but were essential to form a T_{CM} compartment (*22*), confirming that the capability of *Tcf7*$^+$ cells to yield T_{EM} cells ceases over time.

Last, we analyzed the data for evidence that *Tcf7*$^-$ cells reacquired *Tcf7* expression during the expansion or the maintenance phase. Control *Tcf7*$^{GFP+}$ cells expanded 7.6-fold from d6 to d8 p.i., very similar to that of residual *Tcf7*-expressing *Tcf7*$^{DTR\text{-}GFP}$ cells in DT-treated mice. Moreover, the abundance of these *Tcf7*$^+$ cells did not change between d8 and d16 p.i. (Fig. 3J). There was thus no evidence that *Tcf7*$^-$ cells reacquired *Tcf7* expression, indicating that the *Tcf7* locus in d4 *Tcf7*$^-$ cells was stably silenced.

Low TCR and inflammatory signaling favor T_{pCM} relative to T_{TE} formation

Our data suggested that signals early in the immune response determined whether CD8$^+$ T cells maintained or down-regulated the expression of *Tcf7*. To identify signals that could be responsible for modulating early responding CD8$^+$ T cells, we used our scRNA-seq data to evaluate the enrichment of Pathway Interaction Database (PID) (*33*) and Hallmark (*34*) pathway genes in *Tcf7*$^+$ or *Tcf7*$^-$ cells. Compared with T_N cells, CD8$^+$ T cells from d2 p.i., which were essentially all *Tcf7*$^+$, were enriched for the IFN-α, IL-12 (PID), and CD8_TCR downstream pathways (Fig. 4A) However, the TCR_pathway (PID) signature, which includes genes coding for components of the TCR complex (*CD3e*, *CD3g*, and *Lck*), was down-regulated (Fig. 4A), consistent with cells undergoing TCR stimulation (*35*). Down-regulation of the TCR_pathway was less profound in d3 cells and no longer observed in d4 *Tcf7*$^+$ cells. In

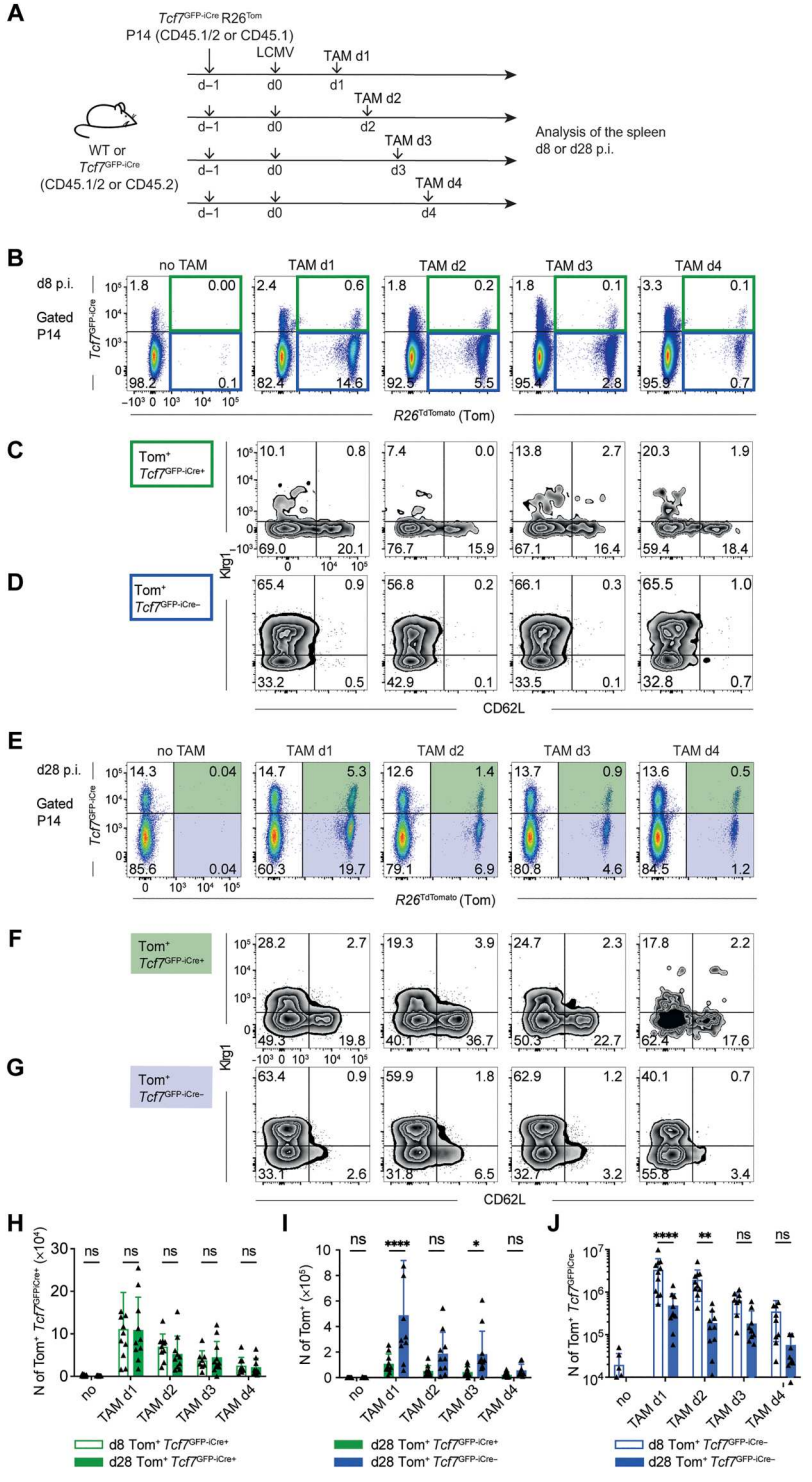

Fig. 2. Fate of *Tcf7*$^{+}$ CD8^{+} T cells during the primary response to infection. (**A**) *Tcf7*$^{GFP\text{-}iCre}$ *R26*^{Tom} P14 cells (CD45.2 or CD45.1/2) were adoptively transferred into B6 (CD45.2 or CD45.1/2) or B6 *Tcf7*$^{GFP\text{-}iCre}$ (CD45.2) mice and infected with LCMV WE 1 day later. Recipient mice were either left untreated (no TAM) or injected with a single dose of TAM on d1 (TAM d1), d2, d3, or d4 p.i. Gated P14 cells present in the spleen were analyzed for the expression of Tom (*R26*^{Tom}) versus GFP (*Tcf7*$^{GFP\text{-}iCre}$). (**B**) d8 Tom^{+} *Tcf7*$^{GFP\text{-}iCre+}$ cells are highlighted in green (open), and d8 Tom^{+} *Tcf7*$^{GFP\text{-}iCre–}$ cells are highlighted blue (open). (**C** and **D**) CD62L versus Klrg1 within these subsets at d8. (**E**) d28 Tom^{+} *Tcf7*$^{GFP\text{-}iCre+}$ cells are highlighted green (filled), and d28 Tom^{+} *Tcf7*$^{GFP\text{-}iCre–}$ cells are highlighted in blue (filled). (**F** and **G**) CD62L versus Klrg1 within these subsets at d28 p.i. (**H**) Number (N) of Tom^{+} *Tcf7*$^{GFP\text{-}iCre+}$ cells at d8 compared with d28 p.i. (**I**) Number of Tom^{+} *Tcf7*$^{GFP\text{-}iCre+}$ compared with Tom^{+} *Tcf7*$^{GFP\text{-}iCre–}$ cells at d28. (**J**) Number of Tom^{+} *Tcf7*$^{GFP\text{-}iCre–}$ cells at d8 compared with d28 p.i. Data in (B) to (J) are compiled from three independent experiments with a total of $n = 6$ to 9 mice per group. Data points in (H) to (J) represent individual mice. Bar graphs show means (±SD). Statistics in (H) to (J) are based on two-way ANOVA with Fisher LSD test, whereby ****$P < 0.0001$; **$P < 0.01$; *$P < 0.05$; and ns, $P > 0.05$.

comparison, the down-regulation of the TCR_pathway was stronger and more sustained in *Tcf7*$^{-}$ cells (Fig. 4A) compared with T_N cells. Thus, these data suggest that *Tcf7*$^{+}$ CD8^{+} T cells are transiently exposed to TCR and inflammatory signals.

The quantity and the quality of TCR signals determine the expansion of antigen-specific cells (*36*, *37*). To address the role of antigen dose and TCR affinity in T_{pCM} formation, we used LCMV cl13 virus strains harboring altered gp33 epitopes. For example, the P14 TCR has no measurable affinity for the F38L (KAVYN**L**ATC) (Δgp33) epitope (*38*), whereas the affinity for the A39C epitope is about 100-fold reduced compared with the wild-type (WT) epitope (*39*). WT mice harboring P14 cells were infected with mixtures of WT and F38L (Δgp33) LCMV cl13 that ranged from 100, 30, 10, 3, to 0% of WT virus (Fig. 4B). The total infectious

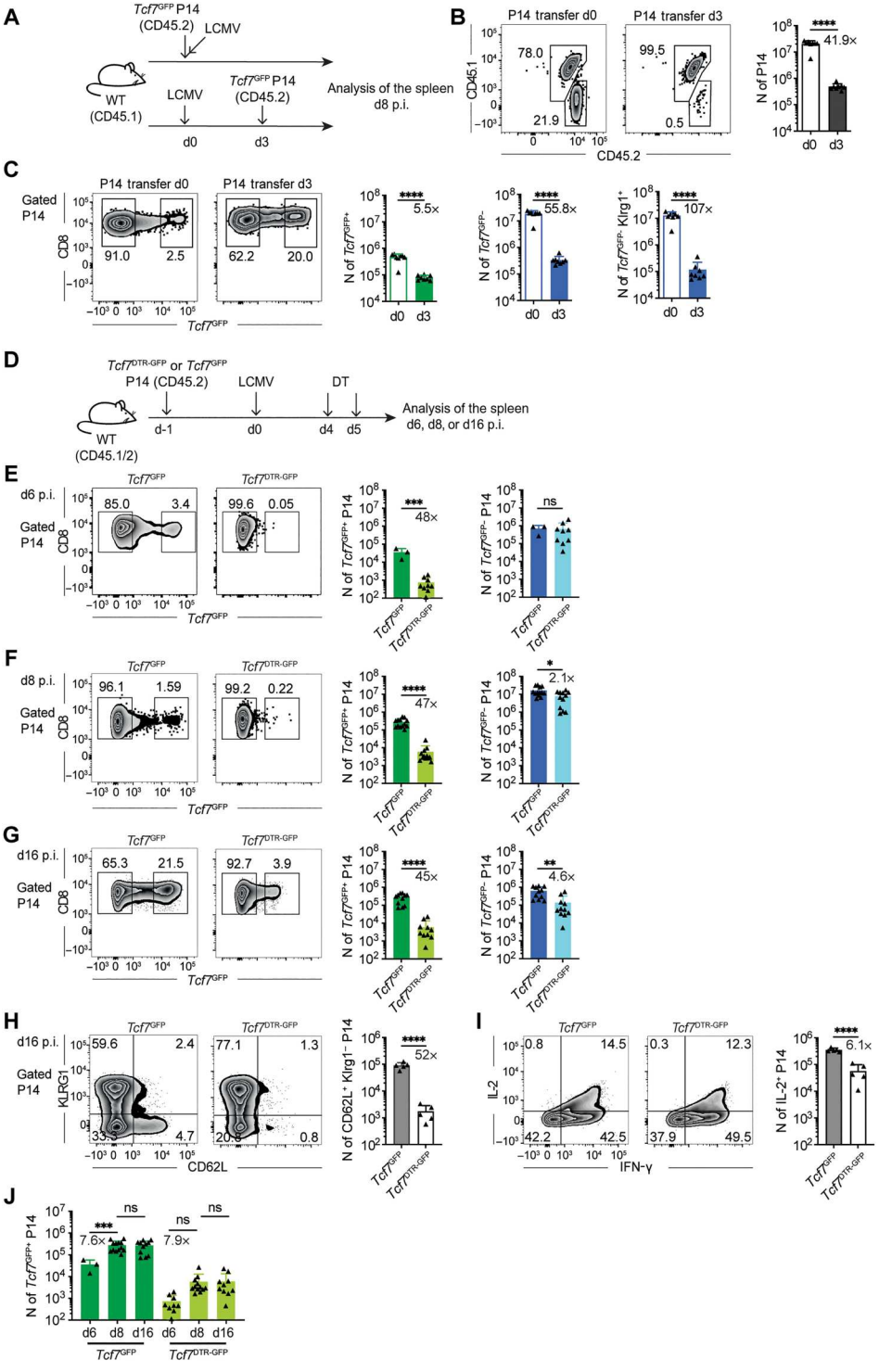

Fig. 3. Progressively limited differentiation of *Tcf7*$^+$ CD8$^+$ T cells during the primary immune response. (**A**) *Tcf7*^{GFP} P14 cells (10^4) (CD45.2) were transferred into B6 mice (CD45.1/2) and infected with LCMV Arm on the same day (P14 transfer d0). Alternatively, recipient mice were infected 3 days before the transfer of *Tcf7*^{GFP} P14 cells (P14 transfer d3) Recipient mice were analyzed on d8 p.i. for (**B**) the number of P14 cells and (**C**) the number of *Tcf7*$^{GFP+}$, *Tcf7*$^{GFP-}$ and *Tcf7*$^{GFP-}$ Klrg1$^+$ P14 cells. (**D**) B6 mice (CD45.1/2) were transferred with *Tcf7*$^{DTR-GFP}$ or *Tcf7*^{GFP} P14 cells (CD45.2) and infected with LCMV Arm one day later. Recipient mice were injected with DT on d4 and d5 p.i. Gated P14 cells were analyzed for the numbers of GFP$^+$ (*Tcf7*$^{DTR-GFP+}$ or control *Tcf7*$^{GFP+}$) cells on (**E**) d6, (**F**) d8, or (**G**) d16 p.i. (**H**) P14 cells were analyzed for the expression of CD62L versus Klrg1 at d16 p.i. The bar graphs show the numbers of CD62L$^+$ Klrg1$^-$ P14 cells at d16 p.i. (**I**) The bar graphs show the numbers of IL-2$^+$ P14 cells at d16 p.i. (**J**) Numbers of GFP$^+$ (*Tcf7*$^{DTR-GFP+}$ or control *Tcf7*$^{GFP+}$) P14 cells on d6, d8, and d16 p.i. Data in (A) to (C) are compiled from two independent experiments with a total of $n = 8$ mice per group. Data in (D) to (J) were compiled from two independent experiments with a total of $n = 5$ to 12 mice per group. Data points in (B), (C), and (E) to (J) represent individual mice. Bar graphs show means (±SD). Statistics is based on unpaired two-tailed Student's *t* test (B, C, and E to I) or one-way ANOVA with Fisher's LSD test (J), whereby ****$P < 0.0001$; ***$P < 0.001$; **$P < 0.01$; *$P < 0.05$; and ns, $P > 0.05$.

dose was kept low (200 PFU) to obtain resolved infection and constant to provide comparable infectious and inflammatory environments. The mixtures induced very similar endogenous CD8$^+$ T cell responses to the np396 epitope (fig. S9A). As expected, P14 cells did not respond to infection with the F38L virus. Progressively increasing the contribution of WT virus to the mixture resulted in a proportional increase in the abundance of P14 cells at d8 p.i. (Fig. 4C). At the lowest antigen dose (3%), the fraction of *Tcf7*$^+$ cells among the total pool of P14 cells was increased (Fig. 4D), and, consequently, that of *Tcf7*$^-$ cells was decreased. Despite minor differences, the responding P14 subsets had comparable phenotypes (fig. S9, B and C), indicating that T_{PCM} formation was less sensitive to a low antigen dose compared with T_{TE} formation. Infection with the LCMV variant expressing the low affinity A39C

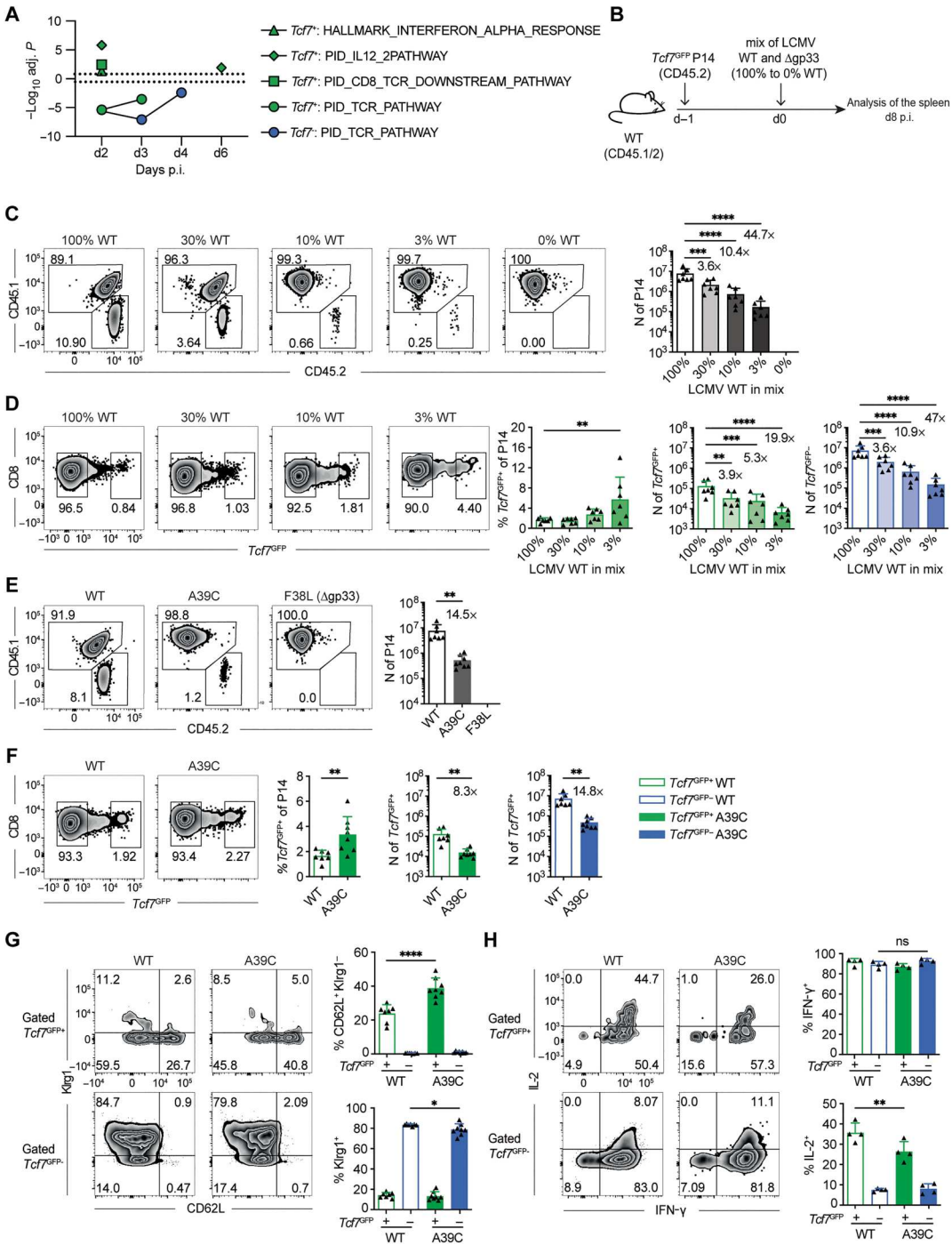

Fig. 4. Low TCR input disfavors T_{TE} relative to T_{pCM} formation. (**A**) Genes differentially expressed between T_N and *Tcf7*$^+$ or *Tcf7*$^-$ cells present at the different time points of infection (based on the scRNA-seq analysis) were subjected to overrepresentation analysis using the PID and the Hallmark (H) gene set collections. The graph shows the significance ($-\log_{10}$ of adjusted *P* values) for the indicated gene sets. For graphical representation, the $-\log_{10}$(adj. *P* value) of gene sets down-regulated in *Tcf7*$^+$ or *Tcf7*$^-$ cells versus T_N cells was multiplied by −1. The dotted line depicts the limit of statistical significance [i.e., $\pm\log_{10}$(0.05)]. (**B**) B6 mice (CD45.1/2) were adoptively transferred with naïve *Tcf7*^{GFP} P14 cells (CD45.2) and infected with a fixed but low dose of WT and Δgp33 (F38L) LCMV cl13, whose gp33 epitope has no measurable affinity for the P14 TCR. The mixtures ranged from 100, 30, 10, 3, to 0% of WT virus. (**C**) Number of P14 cells and (**D**) of *Tcf7*$^{GFP+}$ and *Tcf7*$^{GFP-}$ P14 cells at d8 p.i. (**E** to **H**) B6 mice (CD45.1 or CD45.1/2) were adoptively transferred with naïve *Tcf7*^{GFP} P14 cells (CD45.2) and infected with a fixed low dose of WT, F38L (Δgp33), or A39C LCMV cl13, whose gp33 epitope has a low affinity for the P14 TCR. (E) Number of P14 cells and (F) frequency and number of *Tcf7*$^{GFP+}$ and *Tcf7*$^{GFP-}$ P14 cells at d8 p.i. (G and H) Gated *Tcf7*$^{GFP+}$ and *Tcf7*$^{GFP-}$ cells were analyzed for (G) CD62L versus Klrg1 expression or (H) IL-2 versus IFN-γ production. The data in (B) to (H) were compiled from two independent experiments with a total of $n = 7$ or 8 mice per group. Data in (H) are from a single experiment with of $n = 4$ mice per group. Data points in (C) to (H) represent individual mice. Means (±SD) are shown. Statistics are based on one-way ANOVA with Fisher's LSD test (C to E, G, and H) or nonpaired two-tailed Student's *t* test (F) with ****$P < 0.0001$; ***$P < 0.001$; **$P < 0.01$; *$P < 0.05$; and ns, $P > 0.05$.

epitope resulted in a 14.5-fold reduced expansion of P14 cells (Fig. 4E) that harbored an increased fraction of *Tcf7*$^{GFP+}$ cells compared with the infection with WT LCMV (Fig. 4F). Despite some differences, the responding P14 subsets had a comparable phenotype (Fig. 4, G and H). In addition, the different virus variants induced a similar response by endogenous np396-specific CD8$^+$ T cells (fig. S9D). Thus, the formation of T_{pCM} cells was less affected by low antigen dose and affinity than the generation of T_{TE} cells.

We then investigated how T_{pCM} formation was influenced by inflammatory signals. Exposure to IL-2, IL-12, and IFN-I provides survival factors and promotes effector differentiation (*8*, *14*, *40*). Because IFN-I, rather than IL-12, is essential for effector differentiation in response to LCMV infection (*41*, *42*), we addressed the

importance of signaling through the interferon α/β receptor (IFNAR) in T_{pCM} formation. IFNAR blockade resulted in 15.2-fold reduction of P14 cells, whereby *Tcf7*$^{GFP-}$ and *Tcf7*$^{GFP-}$ Klrg1$^+$ T_{TE} cells were reduced 23.7-fold and 293-fold, respectively. In contrast, the abundance of *Tcf7*$^{GFP+}$ cells was unaltered (Fig. 5, A and B). Although these cells showed normal CD62L expression, IL-2 production was reduced (Fig. 5, C and D). In addition, PD-1 (programmed cell death protein 1) and Lag3 expression was increased compared with controls (fig. S9E). The latter may be related to the fact that IFNAR blockade augments LCMV loads and delays viral clearance (*43*). However, the protracted infection does not account for the lack of Klrg1$^+$ cells, because such cells are readily observed at d8 after LCMV cl13 infection (*44*). These

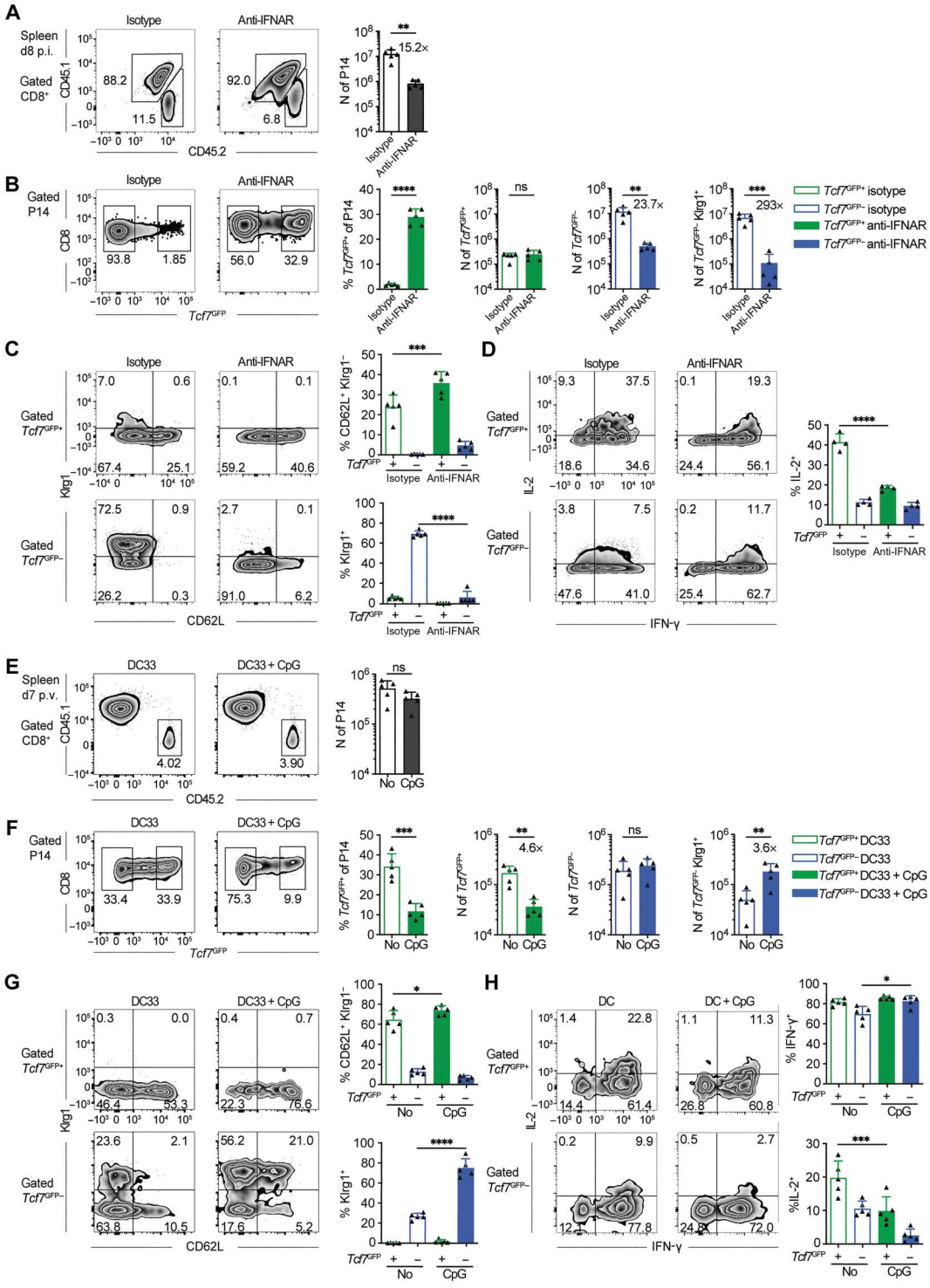

Fig. 5. Inflammatory signaling is dispensable for T_{pCM} formation. (A to D) B6 mice (CD45.1/2) were adoptively transferred with naïve *Tcf7*^{GFP} P14 cells (CD45.2) and infected with LCMV Arm 1 day later (d0). Recipient mice were treated with anti-NK1.1 (to deplete NK cells) and anti-IFNAR or isotype control Ab at d-1. (**A**) Number of P14 cells and (**B**) frequency and number of *Tcf7*$^{GFP+}$, *Tcf7*$^{GFP-}$ and *Tcf7*$^{GFP-}$ Klrg1$^+$ P14 cells at d8 p.i. (**C** and **D**) Gated *Tcf7*$^{GFP+}$ and *Tcf7*$^{GFP-}$ cells were analyzed for (C) CD62L versus Klrg1 expression or (D) IL-2 versus IFN-γ production. (E to H) B6 mice (CD45.1) adoptively transferred with *Tcf7*^{GFP} P14 cells (10^4) (CD45.2) were vaccinated with LPS-matured and gp33 peptide pulsed DC (DC33) without or with TLR9 ligand CpG-B (DC33 + CpG). (**E**) Number of P14 cells and the frequency and number of (**F**) *Tcf7*$^{GFP+}$, *Tcf7*$^{GFP-}$, and *Tcf7*$^{GFP-}$ Klrg1$^+$ P14 cells at d7 postvaccination (p.v.). (**G** and **H**) Gated *Tcf7*$^{GFP+}$ and *Tcf7*$^{GFP-}$ cells were analyzed for (G) CD62L versus KLRG1 expression or (H) IL-2 versus IFN-γ production. Data in (A) to (C) were compiled from two independent experiments with a total of $n = 5$ mice per group. Data in (D) are from a single experiment with $n = 4$ mice per group. Data in (E) to (H) are from one experiment of two performed, each with $n = 3$ to 5 mice per group. Data points in (A) to (H) represent individual mice. Means (±SD) are shown. Statistics are based on nonpaired two-tailed Student's *t* test (A, B, E, and F) or one-way ANOVA with Fisher's LSD test (C, D, G, and H) with ****$P < 0.0001$; ***$P < 0.001$; **$P < 0.01$; *$P < 0.05$; and ns, $P > 0.05$.

data showed that IFN-I signaling was essential for T_{TE} but dispensable for T_{pCM} formation.

T_{pCM} cells are generated in response to dendritic cell vaccination

As a complementary approach to address the role of inflammatory signals in the formation of T_{pCM}, we investigated their generation in response to dendritic cell (DC) vaccination. Mice adoptively transferred with *Tcf7*^{GFP} P14 cells were vaccinated with lipopolysaccharide (LPS)–matured and gp33 peptide-pulsed DC (termed DC33) alone or in combination with systemic exposure to the TLR9 ligand CpG-B (DC33 + CpG) to induce systemic inflammation (*13*, *45*). DC33 and DC33 + CpG vaccination induced a comparable expansion of P14 cells at d7 after vaccination (Fig. 5E) consistent with previous work (*20*, *45*). In response to DC33 + CpG vaccination, most P14 cells had a *Tcf7*$^{GFP-}$ Klrg1^{+} phenotype, but 10% were *Tcf7*$^{GFP+}$ (Fig. 5, F and G). In comparison, DC33 vaccination generated fewer Klrg1^{+} *Tcf7*$^{GFP-}$ and more *Tcf7*$^{GFP+}$ cells (Fig. 5, F and G). There was a similar frequency of CD62L-expressing cells within the *Tcf7*$^{GFP+}$ CD8^{+} T cell population in both vaccination conditions; however, the frequency of IL-2–producing cells was reduced after DC33 + CpG vaccination (Fig. 5, G and H). Thus, the absence of systemic inflammation resulted in an increased generation of cells with a T_{pCM} phenotype in response to DC vaccination.

DC33 vaccination expanded T_{pCM} cells about 200-fold relative to the input of naïve P14 cells (Fig. 5F), which was very similar to the response to LCMV infection (Fig. 1F). In comparison, vaccination with gp33 peptide or gp33 peptide plus adjuvant [polyinosinic:polycytidylic acid (pIC)] did not expand *Tcf7*$^{GFP+}$ P14 cells [showing signs of antigen exposure (CD44^{+})] relative to input (fig. S9F). Although the requirements to generate T_{pCM} cells appeared less stringent than for T_{TE} cells, certain vaccination approaches failed to efficiently yield T_{pCM} cells.

Inflammatory signals received after priming, and once cells have committed to cell division, contribute to TCF1 down-regulation in CD8^{+} T cells

We next investigated the relative importance of priming versus inflammatory cues during the early immune response to commit cells to divide and down-regulate TCF1. CellTrace Violet (CTV)–labeled P14 cells were undivided, and TCF1 protein was expressed at high levels 2 days after infection, but cell division and down-regulation of TCF1 had occurred by d3.5 p.i. (Fig. 6B and fig. S10A). At this time point, we observed nondivided TCF1^{+}, TCF1^{+} cells that had undergone 1 to 3 and >3 divisions, as well as TCF1^{-} cells that had divided >3 times (Fig. 6B), in agreement with previous work (*21*).

To address the importance of inflammation in TCF1 down-regulation and cell division, we treated mice with anti-IFNAR before adoptive cell transfer and infection. When IFNAR was blocked, all cells were divided (Fig. 6B), which is likely explained by augmented viral antigen load (*46*). In addition, IFNAR blockade increased the fraction of highly divided (>3 divisions) TCF1^{+} relative to TCF1^{-} cells (Fig. 6B), suggesting that IFN-I promoted the down-regulation of TCF1 in dividing cells. Cell division has been shown to be necessary for TCF1 down-regulation based on in vitro experiments (*20*, *21*).

We next addressed whether TCF1 expression and cell division were affected by IFN-I exposure during the priming and/or the cell division phase. P14 cells were primed in vivo and flow-sorted on d2 p.i. when cells were undivided and expressed high levels of TCF1. Sorted cells were then cultured in vitro in the absence of additional signals except for the addition of naïve spleen cells and low-dose IL-2 to ensure survival (Fig. 6C). After 48 to 72 hours of culture, P14 cells had undergone 0 to >4 cell divisions, whereby all cells retained high TCF1 levels (Fig. 6D). TCF1 expression also remained high in cells primed in vivo in the presence of anti-IFNAR despite the fact that most P14 cells were divided (Fig. 6, D and F). Thus, priming committed cells to divide multiple times but did not program TCF1 down-regulation. Yet, addition of IFN-β during in vitro culture induced TCF1 down-regulation in dividing cells (Fig. 6, E and F). This was also observed when cells had been primed in the absence of IFNAR signaling (Fig. 6, E and F). Similarly, when naïve P14 cells were activated with gp33 peptide-pulsed splenocytes in vitro, the presence of IL-12 during the division rather than the priming phase down-regulated TCF1 (fig. S10C). Thus, the exposure of primed cells to inflammatory cytokines during the cell division phase was sufficient to induce TCF1 down-regulation.

The absence of TCF1 increases the cycling of CD8^{+} T cells

There is a disparity between the relatively high number of T_{TE} and smaller numbers of T_{pCM} generated during a primary immune response, which has been previously linked to relative rates of cell proliferation (*25*). Consistent with previous work, we observed that T_{CM}-prone TCF1^{+} cells underwent fewer divisions than effector-prone TCF1^{-} cells (Fig. 6B, left) (*21*). This raised the possibility that TCF1 protein itself limited the division of T_{CM}-prone cells. To address this issue, we crossed *Tcf7*^{GFP} reporter transgenic P14 mice to a *Tcf7*$^{-/-}$ background. Naïve P14 cells from these so-called KO *Tcf7*^{GFP} mice expressed the *Tcf7*^{GFP} reporter at high levels (*22*) and were thus useful to track *Tcf7*$^{+}$ (T_{pCM}) cells lacking TCF1 protein. At d3.5 p.i., WT and KO *Tcf7*^{GFP} cells had expanded comparably (Fig. 6, G and H), and subsets of both types of P14 cells retained *Tcf7*^{GFP} expression (Fig. 6I). Although few WT *Tcf7*$^{GFP+}$ cells had divided >3 times, most KO *Tcf7*$^{GFP+}$ cells had divided >3 times (Fig. 6J). In contrast, all WT and KO *Tcf7*$^{GFP-}$ cells had divided >3 times (Fig. 6J).

We further evaluated the division of KO *Tcf7*^{GFP} cells at d4 and at d6 p.i using 5-ethynyl-2′-deoxyuridine (EdU) incorporation during a 2-hour pulse. WT and KO *Tcf7*$^{GFP-}$ cells showed comparable frequencies of EdU^{+} cells, which were increased compared with *Tcf7*$^{GFP+}$ cells (fig. S10D). There were more KO *Tcf7*$^{GFP+}$ cells incorporating EdU than WT *Tcf7*$^{GFP+}$ cells (fig. S10D). Thus, *Tcf7*$^{+}$ cells lacking TCF1 protein underwent more cell divisions, suggesting that the accelerated cycling of *Tcf7*$^{-}$ cells is directly coupled to the down-regulation of TCF1. These data are consistent with a role of TCF1 protein in limiting cell cycle entry or progression, providing an explanation for the preferential expansion of the *Tcf7*$^{-}$ T_{TE} compartment in response to infection.

Stable loss of the T_{pCM} gene signature occurs upon *Tcf7* down-regulation and precedes stable acquisition of a T_{TE} gene signature

To obtain further insights into how the generation of T_{TE} cells from *Tcf7*$^{+}$ cells was controlled, we computed a T_{TE} gene signature score derived from published data of d7 Klrg1^{+} versus d7 Klrg1^{-} cells (*47*) that was characterized by high expression of the genes of interest *Zeb2*, *CX3CR1*, *Klrg1*, and *S1pr5* (Fig. 7, A and B, and data file S2). We compared the distribution of T_{TE} versus the previously

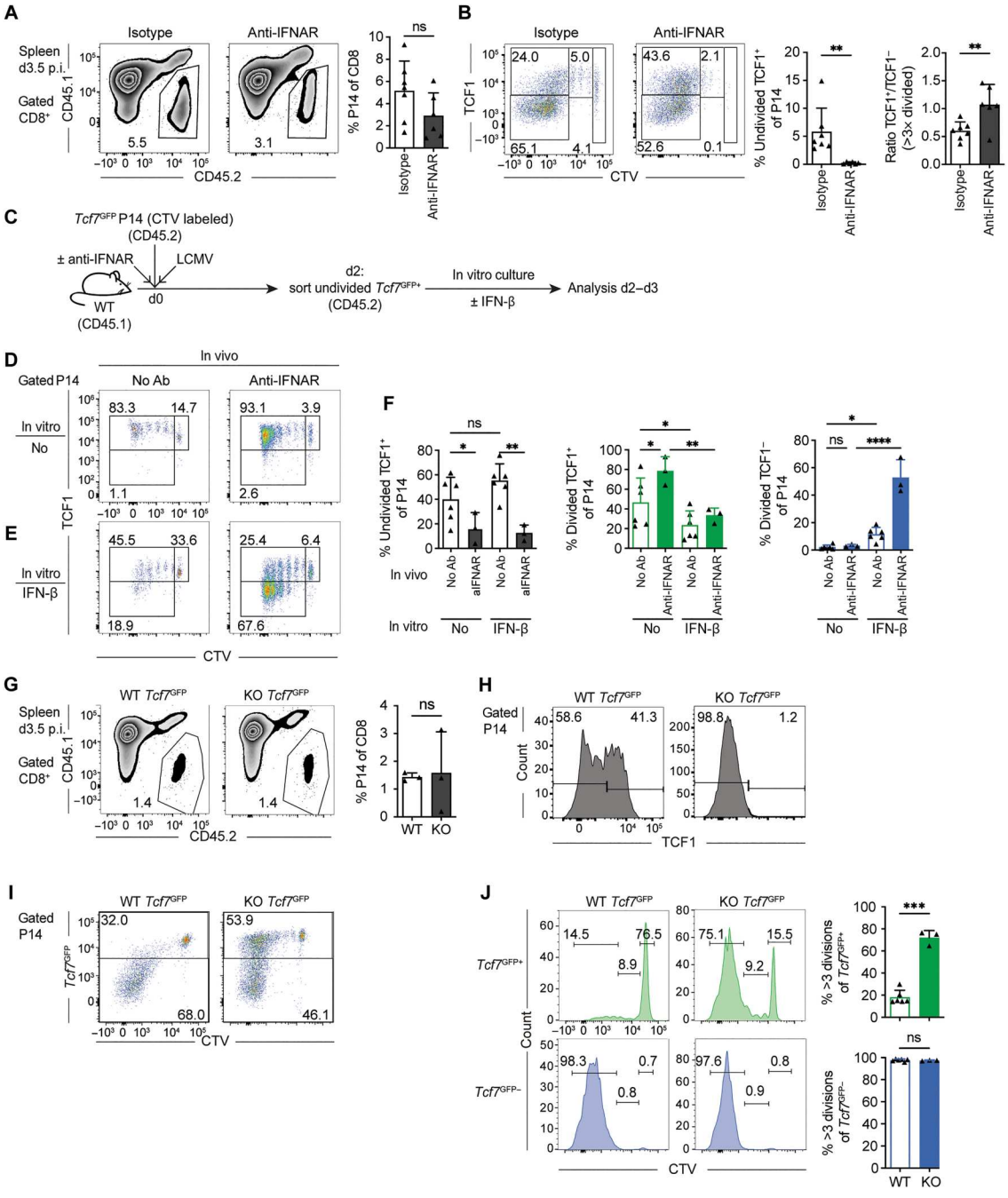

Fig. 6. Role of priming and inflammatory signals in CD8$^+$ T cell cycling and TCF1 down-regulation. (**A** and **B**) B6 mice (CD45.1) were depleted of NK cells, treated with isotype control or anti-IFNAR, transferred with CTV-labeled P14 cells (CD45.2) (10^6), and infected with LCMV WE. (A) Frequency of P14 cells on d3.5 p.i. (B) Gated P14 cells were analyzed for CTV versus TCF1, discriminating between undivided TCF1$^+$ cells, low divided TCF1$^+$ cells (one to three divisions), high divided TCF1$^+$ cells (>3 divisions), and high divided TCF1$^-$ cells (>3 divisions). The bar graphs show the fraction of undivided TCF1$^+$ cells (left) and the ratio of TCF1$^+$ versus TCF1$^-$ cells that had divided >3 times (right). (**C** to **F**) B6 mice (CD45.1) were treated with anti-IFNAR, transferred with CTV-labeled P14 cells (CD45.2) (10^6), and infected with LCMV WE on d0. Undivided P14 cells were flow-sorted on d2 p.i. and cultured in vitro in the presence or absence of IFN-β for 2 to 3 days. (D and E) Gated P14 cells were analyzed for CTV versus TCF1. Gates discriminate between undivided TCF1$^+$ cells, divided TCF1$^+$ cells, and divided TCF1$^-$ cells. (F) Fraction of undivided TCF1$^+$ cells (left), divided TCF1$^+$ cells, and divided TCF1$^-$ cells from (D) and (E). (**G** to **J**) B6 mice (CD45.1) were transferred with CTV-labeled WT or *Tcf7* KO *Tcf7*^{GFP} P14 cells (CD45.2) (10^6) and infected with LCMV WE. (G) Frequency of P14 cells on d3.5 p.i. Gated P14 cells were analyzed for (H) TCF1 and (I) CTV versus *Tcf7*^{GFP}. (J) Gated *Tcf7*$^{GFP+}$ and *Tcf7*$^{GFP-}$ cells were analyzed for CTV. Gates distinguish between undivided, divided (one to three divisions), and highly divided cells (>3 divisions), with the frequencies of highly divided cells in each subpopulation shown in graphs alongside. (A and B) Data were compiled from three independent experiments with a total of $n = 6$ or 7 mice per group. (C to F and G to J) Data are compiled from two independent experiments with a total of $n = 3$ to 6 mice per group. Data points in (A), (B), (G), and (J) represent individual mice or (F) cultures derived from individual mice. Means (±SD) are shown. Statistics are based on non-paired two-tailed Student's *t* test (A, B, G, and J) and one-way ANOVA with Fisher's LSD test (F) with ****$P < 0.0001$; ***$P < 0.001$; **$P < 0.01$; *$P < 0.05$; and ns, $P > 0.05$. KO, knockout.

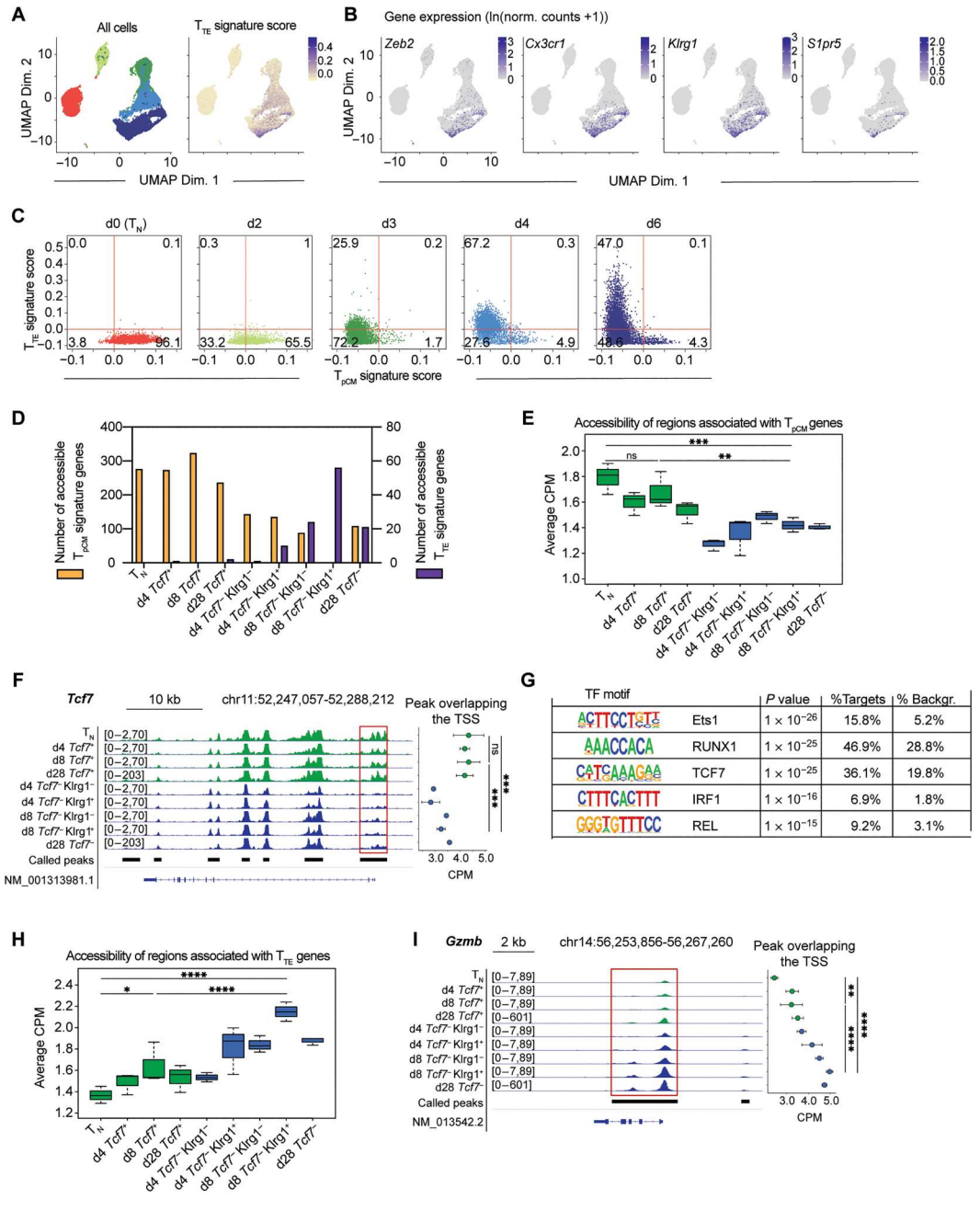

Fig. 7. Stable loss of the T_{pCM} gene signature occurs upon *Tcf7* down-regulation and precedes stable acquisition of a T_{TE} gene signature. B6 mice (CD45.1) were adoptively transferred with naïve *Tcf7*^{GFP} P14 cells (CD45.2) and infected with LCMV Arm. (A to C) P14 cells (CD45.2) cells were flow-sorted on d2, d3, d4, and d6 p.i. and, together with naïve P14 cells (T_N), subjected to scRNA-seq. (**A**) UMAP plot of P14 cells colored according to the time point p.i. (left) (described in Fig. 1A) and according to their T_{TE} signature score (right), derived as described in Materials and Methods. (**B**) Expression of selected T_{TE} genes [ln (norm. counts + 1)] by individual P14 cells. (**C**) Individual P14 cells colored according to the time point p.i. (described in Fig. 1A) were analyzed for the overall intensity of the T_{TE} versus the T_{pCM} signature score. (D to I) *Tcf7*$^{GFP+}$, *Tcf7*$^{GFP-}$ Klrg1$^-$, and *Tcf7*$^{GFP-}$ Klrg1$^+$ P14 cells (CD45.2) were flow-sorted on d4 or d8 p.i. and, together with naïve P14 cells (T_N) and prior data from d28 *Tcf7*$^+$ and d28 *Tcf7*$^-$ memory cells, subjected to bulk ATAC-seq analysis. (**D**) A total of $n = 323$ genes were overexpressed and more accessible in T_{pCM} (d8 *Tcf7*$^+$ compared with d8 *Tcf7*$^-$ cells), and $n = 56$ genes were overexpressed and more accessible in T_{TE} (d8 *Tcf7*$^-$ Klrg1$^+$ compared with d8 *Tcf7*$^+$ cells). The bar graph shows the number of overexpressed and more accessible T_{pCM} signature genes (yellow bars) or T_{TE} signature genes (purple bars) in the indicated populations of *Tcf7*$^+$ and *Tcf7*$^-$ cells. (**E**) The epigenetically regulated T_{pCM} signature genes ($n = 323$) were associated with $n = 876$ more accessible regions. The box plot depicts the average read coverage for these regions indicated as counts per million (CPM) in the indicated populations of cells. (**F** and **I**) Genome browser view of sequencing read coverage (dark blue tracks) at the *Tcf7* (F) and GzmB locus (I). Black horizontal lines depict accessible regions based on peak calling. The dot graphs in (F) and (I) depict means (±SD) of the normalized accessibility of the called peak overlapping the transcriptional start site (TSS) in the different populations ($n = 3$ samples). (**G**) Motif search analysis of regions more accessible in T_{pCM} genes (excluding repetitive regions). (**H**) The epigenetically regulated T_{TE} genes ($n = 56$) were associated with $n = 152$ more accessible regions. The box plot depicts the average read coverage for these regions in the indicated populations of cells. Statistics in (F) and (I) are based on one-way ANOVA with Fisher's LSD test with ****$P < 0.0001$; ***$P < 0.001$; **$P < 0.01$; *$P < 0.05$; and ns, $P > 0.05$.

calculated T_{pCM} signature scores (data file S2) in single CD8$^+$ T cells. The vast majority of d2 cells had a positive T_{pCM} but a negative T_{TE} score (Fig. 7C). Similarly, the vast majority of T_{pCM} score-positive cells at subsequent time points had a negative T_{TE} score (Fig. 7C), indicating that the two signatures rarely coexisted in single cells. Rather, some d2 cells and the majority of the later cells had a negative T_{pCM} score. These T_{pCM}-negative cells lacked a T_{TE} signature at d2, whereas some d3 and most d4 cells had a weak T_{TE} score. Cells with a high T_{TE} score were first observed on d6 (Fig. 7C). Similar data were obtained using T_{CM}- versus T_{EM}-derived signature scores (data file S2 and fig. S11, A and B). Thus, these data suggested that CD8$^+$ T cells first down-regulated the expression of T_{pCM} signature genes before up-regulating T_{TE} signature genes.

We further addressed whether the transcriptional changes were related to changes in chromatin accessibility. To this end, we performed assays for transposase-accessible chromatin with sequencing (ATAC-seq) analysis of *Tcf7*$^+$ (T_{pCM}), *Tcf7*$^-$ Klrg1$^-$, and *Tcf7*$^-$ Klrg1$^+$ (T_{TE}) cells isolated at d4 and d8 p.i. together with T_N cells and d28 *Tcf7*$^+$ (T_{CM}) and d28 *Tcf7*$^-$ cells (T_{EM}). Although the different samples had comparable numbers of accessible regions, the sequencing coverage was lower in d4 *Tcf7*$^-$ cells (fig. S11C). This may be due to the rapid cycling of most d4 cells (fig. S10D), which reduces chromatin accessibility (*48*). To address accessibility changes in T_{pCM} and T_{TE} signature genes, we integrated our bulk ATAC-seq data with previously published bulk RNA-seq data (*22*). Among the T_{pCM} genes overexpressed at the mRNA level (n = 602), n = 323 genes were more accessible in T_{pCM} cells, including the genes of interest *Tcf7*, *Sell*, and *Ccr7* (Fig. 7, D and F; fig. S11D; and data file S3). These genes contained a total of n = 872 regions that were, on average, more accessible in T_{pCM} cells (Fig. 7E). These epigenetically regulated T_{pCM} genes and regions were also accessible in T_N, in d4 *Tcf7*$^{GFP+}$, and in d28 *Tcf7*$^+$ cells (T_{CM}). On the other hand, these genes/regions were less accessible in all *Tcf7*$^{GFP-}$ populations (Fig. 7, D to F). Motif search analysis showed that these less accessible regions were highly enriched for *Tcf7*-binding motifs (Fig. 7G). Thus, a considerable fraction of T_{pCM} genes contained *Tcf7*-binding motifs and became less accessible and less expressed at the time point when *Tcf7* was down-regulated, and this was associated with the loss of stemness.

Conversely, among genes overexpressed in T_{TE} cells (n = 119), n = 56 genes were more accessible in T_{TE} cells, including the genes of interest *Gzmb*, *Klrg1*, *and Fasl* (Fig. 7, D and I; fig S10E; and data file S3). These genes contained a total of n = 152 regions that were more accessible in T_{TE} cells (d8 *Tcf7*$^-$ Klrg1$^+$) (Fig. 7H). The epigenetically regulated T_{TE} genes/regions were poorly accessible in all *Tcf7*$^+$ populations (T_N, d4, d8, and d28). T_{TE} genes/regions were also poorly accessible in d4 *Tcf7*$^{GFP-}$ Klrg1$^-$ cells but gained some accessibility in the occasional d4 *Tcf7*$^{GFP-}$ Klrg1$^+$ (fig. S1F) and in d8 *Tcf7*$^{GFP-}$ Klrg1$^-$ cells but reached maximal accessibility only in d8 *Tcf7*$^{GFP-}$ Klrg1$^+$ (T_{TE}) cells (Fig. 7, D, H, and I, and fig. S10E). The accessibility of T_{TE} genes in d28 *Tcf7*$^-$ (T_{EM}) cells was intermediate and corresponded to that seen in the d8 *Tcf7*$^{GFP-}$ Klrg1$^-$ population (Fig. 7H). Many of these latter cells correspond to CD127$^+$ Klrg1$^-$ cells, i.e., MPEC from which *Tcf7*$^+$ cells had been excluded (fig. S2B), suggesting that T_{EM} cells mainly derive from d8 *Tcf7*$^-$ CD127$^+$ Klrg1$^-$ cells. Although T_{TE} genes were expressed in d4 *Tcf7*$^-$ cells, these genes became fully accessible only in *Tcf7*$^-$ Klrg1$^+$ cells at d8 p.i. On the other hand, the *Ifng* locus was comparably accessible in *Tcf7*$^+$ and *Tcf7*$^-$ cells of the same time point but was poorly accessible in T_N cells (fig. S10F), in agreement with IFN-γ production (fig. S2C). The *Ifng* locus, thus, seemed to become accessible in response to activation and independent of T_{pCM}/T_{TE} differentiation. We concluded that the stable loss of stemness as seen in d4 *Tcf7*$^-$ cells preceded the stable acquisition of a T_{TE} program during CD8$^+$ T cell differentiation.

DISCUSSION

The stage of an acute immune response when T cells commit to long-lived T_{CM} cells or to terminally differentiated effector cells has remained controversial. Here, we showed that a small population of TCF1$^+$ CD8$^+$ T cells with stem cell–like potential and T_{CM} precursor function was present throughout the primary response to infection. These TCF1$^+$ cells derived directly from primed naïve T cells, whereby their expansion was proportional to the TCR signaling strength but independent of IFNAR signaling during infection or independent of systemic inflammation during DC vaccination. These findings are in line with earlier work showing that a brief stimulation of naïve CD8$^+$ T cells with antigen plus costimulation is sufficient for T_{CM} formation (*49*, *50*), and DC vaccination in the absence of systemic inflammation results in accelerated T_{CM} formation (*13*). Thus, the default fate in response to T cell activation is the generation of TCF1$^+$ cells, which act as precursors of T_{CM} cells.

Prior work showed that T_{CM} cells preferentially derive from MPEC (CD127$^+$ Klrg1$^-$ effector cells), which have cytolytic activity (*8*, *51*). To generate nonlytic T_{CM} cells, some MPEC would have to dedifferentiate, i.e., lose lytic activity, and acquire stem-like properties after pathogen clearance (*6*–*8*, *12*, *51*). This linear differentiation scheme is supported by epigenetic changes of the *Sell* locus (encoding CD62L), which is demethylated in T_N cells but has inhibitory DNA methylation marks in MPEC [and in short-lived effector cells (CD127$^-$ Klrg1$^+$)] and is again demethylated in T_{CM} cells (*7*). Similarly, the *Gzmb* locus is poorly accessible in T_N cells but is comparably accessible in MPEC and SLEC as well as in unfractionated memory cells (*52*–*54*). This suggested that all cells acquire an "effector-like" epigenetic program and that dedifferentiation of some MPECs was needed for T_{CM} formation.

We recently reported that T_{CM} cells derive from d8 *Tcf7*$^+$ CD8$^+$ T cells, which represent a subset of about 10% of MPEC. These *Tcf7*$^+$ cells lack lytic activity and already have stem cell–like properties (*22*). However, because pathogen control is essentially complete at the peak of the primary response, it was possible that the d8 *Tcf7*$^+$ cells exist in the absence of antigen and that dedifferentiation has already occurred. Here, we showed that *Tcf7*$^+$ cells displaying T_{pCM} function and stem-like properties are present throughout the primary response to infection. Stemness was, thus, maintained in a subset of CD8$^+$ T cells in the presence of antigen rather than acquired subsequent to pathogen clearance. The apparent inconsistency to prior data very likely derives from the fact that only 10% of MPEC are *Tcf7*$^+$ cells. In contrast to MPEC, naïve/central memory genes (*Tcf7*, *Sell*, or *Ccr7*) were accessible in T_{pCM} cells (d4 or d8 *Tcf7*$^+$), similar to T_N cells. Conversely, effector genes (*GzmB*, *Klrg1*, or *FasL*) were poorly accessible in T_{pCM} and T_{CM} cells and only modestly increased compared with T_N cells. These analyses thus suggested that T_{CM} cells derived from precursor cells that maintained stemness and that had not previously acquired a stable effector program. However, earlier work suggested that T_{CM} cells had expressed *GzmB* at some earlier stage (*6*). Some *Tcf7*$^+$ cells expressed GzmB both at the mRNA and protein level until d4 of infection (fig. S2D) (*55*). Despite that, the accessibility of *GzmB* gene body (±5 kb) in T_{pCM} cells (d4 or d8 *Tcf7*$^+$) was only slightly increased compared with T_N cells. Notwithstanding, an element 22 kb upstream of the *GzmB* locus showed considerably increased accessibility in T_{pCM} and T_{CM} cells compared with T_N cells, providing evidence that the *GzmB* locus has been active in T_{CM}-prone cells. These cells did not acquire the chromatin accessibility changes associated with T_{TE} differentiation. The data, thus, suggest that T_{CM} cells derive from *Tcf7*$^+$ precursors without the need for dedifferentiation.

The continuous presence of stem-like cells satisfied a key prediction of the progressive differentiation model. However, the stage

during the immune response when stem-like cells committed to a T_{TE} fate remained unclear. Lineage tracing showed that only the $TCF1^+$ cells present during priming (i.e., before or around the first cell division) were competent to yield $TCF1^-$ T_{TE} cells despite stem-like $TCF1^+$ cells being present throughout the primary immune response. Culturing in vivo primed but undivided $TCF1^+$ cells showed that these cells were programmed to undergo several divisions, as shown before (*56*), whereby TCF1 expression was maintained. Addition of IFN-β during the division phase in vitro induced TCF1 down-regulation, but prior IFNAR signaling in vivo was not needed. Thus, priming produced divided $TCF1^+$ cells that were committed to become T_{CM} cells and that could be diverted toward an effector fate by inflammatory cytokines, which suppressed TCF1. Prior work suggested that the effector versus memory fate decision is made on the basis of a first asymmetric cell division, whereby the DC proximal daughter cell is effector-prone and the distal daughter cells is memory-prone (*9*). Although there was no evidence of asymmetric TCF1 distribution during the first three cell divisions, see also (*21*), it remains possible that the initial cell division generates effector-prone cells. However, such cells may realize their potential only several generations later, dependent on their exposure to inflammatory signals. Thus, priming generates T_{CM}-prone $TCF1^+$ cells, and inflammation-dependent TCF1 down-regulation initiates the diversion of some of these cells toward an effector fate.

Last, we addressed the hierarchy of transcriptional and chromatin accessibility changes associated with differentiation. Previous data suggested that naïve cells, which express a stem/memory signature but lack an effector gene signature, give rise to cycling cells expressing both signatures. Such bipotent differentiation intermediates then commit toward effector cells by silencing the stem/memory signature (*17*). However, this hierarchy was deduced from a relatively late stage of the response to bacterial infection (d7), whereas we obtained evidence for a stable cell fate change on d3.5 to d4 of the response, which occurred upon TCF1 down-regulation. TCF1 loss resulted in a reduced accessibility of the *Tcf7* locus and a subset of T_{pCM} signature genes. TCF1 down-regulation was associated with the loss of T_{pCM} function and stemness and was stable, because there was no evidence that *Tcf7* was reexpressed by $Tcf7^-$ cells. These early $Tcf7^-$ cells had not yet acquired a stable T_{TE} program. Thus, we propose that T_{TE} differentiation involves the stable loss of stemness, which occurs in response to inflammation-induced TCF1 down-regulation, and that this is followed by the stable acquisition of a T_{TE} state.

The current study has some limitations. The early phase of the response was studied using unphysiologically large numbers of virus-specific $CD8^+$ T cells, which reduces cellular activation and could thus explain the presence of $TCF1^+$ $CD8^+$ T cells early during the primary response. However, lineage tracing and lineage deletion experiments are based on lower numbers of input cells, and the findings provide clear, although circumstantial, evidence that $TCF1^+$ $CD8^+$ T cells were present throughout the primary response. Last, the study does not address the question of how some primed cells retain TCF1 in the face of systemic inflammation.

A key goal of understanding the developmental origin of T_{CM} cells is to generate such cells by vaccination. The identification of T_{CM} precursor cells represents an important step toward that goal. Here, we showed that DC vaccination (in the absence of systemic inflammation) leads to a 200-fold expansion of antigen-specific $Tcf7^+$ cells (compared with the input of naïve T cells), which was remarkably similar to LCMV infection. Conversely, peptide plus adjuvant vaccination failed to amplify $Tcf7^+$ cells. These initial experiments highlight that $Tcf7^+$ cells can be expanded by vaccination but that the precise conditions will need to be defined and improved. The identification of $TCF1^+$ T_{pCM} cells should greatly facilitate the optimization of current and the testing of approaches of candidate T cell vaccines.

MATERIALS AND METHODS

Study design

The goal of this study was to understand the developmental origin of effector and memory $CD8^+$ T cells in response to viral infection. TCR transgenic T cells—expressing reporters to isolate, track the fate, or ablate virus-specific $Tcf7^+$ CD8+ T cells—were transferred into congenically distinct hosts, and the response to acutely resolving LCMV infection was characterized by flow cytometry. The potential of expansion-phase $Tcf7^+$ and $Tcf7^-$ $CD8^+$ T cell subsets was examined using recall responses in secondary recipient mice, whereas their fate was addressed using *Tcf7*-guided cell tracing and ablation experiments. These findings were related to transcriptome and chromatin accessibility analyses. Group sizes were $n = 5$ or as indicated in the figure legends, and experiments were repeated at least twice. Occasional mice were excluded for technical reasons, i.e., incomplete intravenous injections.

Mice

C57BL/6 (B6) ($CD45.2^+$) mice were obtained from Envigo (Gannat, France), CD45.1 congenic B6 mice were bred locally, B6 P14 T cell receptor (TCR) transgenic mice (line 237) were provided by H. P. Pircher (Freiburg, Germany) ($CD45.2^+$) (*57*), and $Tcf7^{-/-}$ mice (*58*) were provided by H. Clevers (Utrecht, the Netherlands). Rosa26 lox stop lox Confetti ($R26^{Confetti}$) (*59*) mice were provided by J. Joyce [University of Lausanne (UNIL)]; Rosa26 lox stop lox TdTomato ($R26^{Tomato}$) (*60*) mice were provided by J. Huelsken (EPFL, Switzerland); and $Tcf7^{GFP}$ (*28*), $Tcf7^{DTR\text{-}GFP}$ (*31*), and $Tcf7^{GFP\text{-}CreERT2}$ ($Tcf7^{GFP\text{-}iCre}$) (*22*) mice have been described. P14 $Tcf7^{GFP}$, P14 $Tcf7^{GFP}$ $Tcf7^{-/-}$, P14 $Tcf7^{DTR\text{-}GFP}$, P14 $Tcf7^{GFP\text{-}iCre}$ $R26^{Confetti}$, and P14 $Tcf7^{GFP\text{-}iCre}$ $R26^{Tomato}$ mice were obtained by breeding ($CD45.2^+$ unless indicated otherwise). Experiments used both male and female mice between 6 and 12 weeks of age, whereby donors and recipients of adoptive T cell transfers were sex-matched. Animal experiments were conducted in accordance with protocols approved by the veterinary authorities of the Canton de Vaud (reference numbers VD1124.8 and VD3704).

LCMV infections

Mice were infected with LCMV 53b Armstrong strain (Arm) (2×10^5 PFU, i.p.), LCMV WE strain (200 PFU, i.v.), LCMV clone 13 (cl13) (200 PFU, i.v.), gp33 epitope mutant (F38L) LCMV cl13 (200 PFU, i.v.) (*38*), or gp33 epitope mutant (A39C) LCMV cl13 (200 PFU, i.v.) (*39*). For recall responses, mice were infected with LCMV Arm (2×10^5 PFU, i.p.) or LCMV WE (2000 PFU, i.v.).

Adoptive T cell transfer

P14 cells were obtained by mashing the spleen through a 40-μm nylon cell strainer (BD Falcon). Red blood cells were lysed with a

hypotonic ammonium-chloride-potassium (ACK) buffer. $CD8^+$ T cells were purified using mouse $CD8^+$ T cell enrichment kit (STEMCELL Technologies). Purified P14 cells ($CD45.2^+$ or $CD45.1/2^+$) (usually >95% pure) were adoptively transferred intravenously into naïve B6 ($CD45.2^+$, $CD45.1^+$, or $CD45.1/2^+$) 1 day before infection (d−1). For lineage tracing experiments using $Tcf7^{GFP\text{-}iCre}$ $R26^{Tomato}$ P14 cells ($CD45.1/2^+$), Tom^- cells were flow-sorted and transferred into WT or $Tcf7^{GFP\text{-}iCre}$ recipients ($CD45.2^+$). For the analysis of primary responses, the number of P14 input cells depended on the time point of the analysis: ~0.8×10^6 to 2×10^6 P14 cells for analyses at d2 or d3 p.i. and 10^5 P14 cells for d4 and 10^4 P14 cells for all later time points. For experiments using KO $Tcf7^{GFP}$ cells, $CD62L^+$ $Tcf7^{GFP+}$ P14 cells were flow-sorted from the spleens of naïve mice before transfer into recipients. For some experiments, purified P14 cells were labeled with CTV (2.5 μM) according to manufacturer's instructions. For recall responses, 10^4 flow-sorted P14 cells were transferred and recipients were infected with LCMV on the same day (d0).

Antibody treatment

For natural killer (NK) cell depletion, mice were injected intraperitoneally with anti-NK1.1 (PK136) (0.5 mg). For IFNAR blockade, mice were injected intraperitoneally with anti-IFNAR1 (MAR1-5A3) (1 mg) or isotype control antibody (Ab) (mouse immunoglobulin G1) (MOPC-21). All Abs were purchased from Bio X Cell.

TAM, DT, and EdU treatment

Mice transferred with $R26^{Tomato}$ $Tcf7^{GFP\text{-}iCre}$ P14 cells were injected intraperitoneally with a single dose of 0.1 mg of TAM (T5648, Sigma-Aldrich). Mice transferred with $R26^{Confetti}$ $Tcf7^{GFP\text{-}iCre}$ P14 cells were injected intraperitoneally with 1 mg of TAM on 3 to 4 consecutive days. Induction of Cre activity in $R26^{Confetti}$ cells results in the stochastic and mutually exclusive expression of one of four fluorescent proteins [red fluorescent protein (RFP), cyan fluorescent protein (CFP), yellow fluorescent protein (YFP), or green fluorescent protein (GFP)] (*59*). Here, labeling was followed on the basis of RFP expression. Cre induction also yielded cells expressing high levels of GFP and YFP, which could be discriminated from $Tcf7^{GFP\text{-}iCre+}$ cells based on the intermediate GFP levels of the latter. The GFP/YFP^{hi} cells were excluded from the analysis. Control mice were injected with sunflower vehicle only.

DT (D0564, Sigma-Aldrich) was injected intraperitoneally (50 μg/kg of body weight, i.e., about 1 μg of DT per mouse). Control mice were injected with phosphate-buffered saline (PBS). Mice were injected intraperitoneally with 2 mg of EdU 2 hours before euthanasia.

Cell culture

B6 splenocytes ($CD45.1^+$) were pulsed with gp33-41 peptide (KAVYNFATM) (1 μM) for 1 hour, washed three times, and used to stimulate P14 cells (CD45.2) purified from the spleens of naïve mice. Anti-IL12p40 Ab (1 μg/ml) (C17.8) (Bio X Cell) and/or IL-12 (0.1 to 0.3 μg/ml) (PeproTech) were added as indicated.

P14 cells flow-sorted at d2 p.i. (10^4) were cultured for 48 to 72 hours in the presence of naïve splenocytes (10^4) and low-dose IL-2 (50 ng/ml) (recombinant human, Glaxo, a gift from N. Rufer, UNIL) to ensure survival. Where indicated, IFN-β (1000 U/ml) (BioLegend) was added to the culture.

Vaccination

For DC vaccination, B6 recipient mice ($CD45.1^+$ or $CD45.1^+2^+$) were adoptively transferred with purified P14 $Tcf7^{GFP}$ cells (10^4) ($CD45.2^+$) 1 day before the intravenous injection of bone marrow–derived, LPS-matured, and gp33 peptide-pulsed DC (DC33) (10^6), with or without intraperitoneal injection of 50 μg of CpG-B 1826 oligodeoxynucleotides (TriLink Biotechnologies), as described in detail in (*20*).

For peptide vaccination, purified P14 $Tcf7^{GFP}$ cells (10^6) ($CD45.2^+$) were adoptively transferred 1 day before vaccination. Mice were injected subcutaneously with 50 μg of poly(I:C) (Invivogen) together with gp33 peptide (10 μg) (TCMetrix). Mice were analyzed on day 7 after vaccination.

Tissue preparation and cell suspensions

Spleens were mashed through a 40-μm nylon cell strainer to obtain single-cell suspensions. This was followed by red blood cell lysis using ACK buffer.

For the isolation of IELs, the small intestine was collected, cut into small pieces, and flushed with Hanks' balanced salt solution (HBSS) 2% fetal calf serum (FCS) before excising the Peyer's patches. This was followed by incubation with 1 mM dithiothreitol (AppliChem, A3668) in HBSS 10% FCS for 20 min at 37°C. The cell suspension was filtered using a 100-μm strainer (Falcon) and centrifuged, and $CD8^+$ T cells were enriched using positive selection by magnetic-activated cell sorting (Miltenyi Biotec kit, 130-116-478).

Flow cytometry and cell sorting

Surface staining was performed for 15 min at 4°C in PBS supplemented with 2% FCS (FACS buffer) using the reagents listed in data file S4. For tetramer stainings, cell suspensions were incubated with anti-CD16/32 (2.4G2) hybridoma supernatant before staining for 90 min at 4°C with allophycocyanine-conjugated major histocompatibility complex-I tetramers (data file S4). A Zombie Aqua Fixable Viability kit (BioLegend) was used to exclude dead cells.

For intranuclear staining, cells were surface-stained before fixation and permeabilization using the Foxp3 staining kit (eBioscience, catalog no. 00-5523), followed by intranuclear staining in permeabilization buffer 1× (Perm buffer). For cytokine production, splenocytes were restimulated in vitro with LCMV gp33-41 (gp33) (1 μM) peptide for 5 hours in the presence of brefeldin A (5 μg/ml) for the last 4.5 hours. Cells were surface-stained before fixation and permeabilization (Intracellular Fixation & Permeabilization Buffer Set, eBioscience kit, catalog no. 88–8824), followed by intracellular staining in 1× Perm buffer. For GzmA and GzmB detection, splenocytes were cultured in the absence of peptide but in the presence of brefeldin A (5 μg/ml) for 4.5 hours before intracellular staining as described above.

EdU was detected with the Click-iT Plus EdU Alexa Fluor 488 Imaging Kit (Molecular Probes, Thermo Fisher Scientific) according to the manufacturer's instructions. Flow cytometry measurements of cells were performed on an LSR-II or Fortessa flow cytometer (BD). Data were analyzed using FlowJo (TreeStar).

For cell sorting of P14 cells, splenocytes were enriched for $CD8^+$ T cells using the mouse $CD8^+$ T cell enrichment kit (STEMCELL Technologies) before cell surface staining. Cells were flow-sorted to a purity of >99% (based on post-sort analysis) using a FACSAria (BD) flow cytometer.

scRNA-seq analysis

Purified *Tcf7*^{GFP} P14 cells (CD45.2) were adoptively transferred into B6 (CD45.1) mice before infection with LCMV Arm. P14 cells were flow-sorted from the spleen of one mouse (for d0), pooled spleens of three mice (for d2, d3, or d4), or pooled spleens of two mice (for d6), and one sample per time point was subjected to scRNA-seq analysis as described in Supplementary Methods. After quality control, a total of 19,374 cells were retained for further analysis (data file S1). Genes differentially expressed between d0 (T_N) cells and all cells or *Tcf7*$^+$ cells of each time point were identified using the FindMarkers function in Seurat with default parameters, and overrepresentation analyses of the PID (*33*) and Hallmark (*34*) gene set collections from the Molecular Signature Database (MSigDB) v7.5.1) were performed separately for up- or down-regulated genes using the enricher function of the clusterProfiler package (v3.18.1) (*61*).

Gene signatures and calculation of module scores

T_{pCM} and T_{CM} gene signatures derived from bulk RNA-seq analysis of d8 *Tcf7*$^+$ (T_{pCM}) versus d8 *Tcf7*$^-$ P14 cells and d30 *Tcf7*$^+$ (T_{CM}) versus d30 *Tcf7*$^-$ P14 cells (T_{EM}) after LCMV Arm infection (*22*). Genes were considered differentially expressed when [$\log_2$(fold change) > 2] and are listed in data file S2. A T_{TE} signature was generated using publicly available bulk RNA-seq data of Klrg1$^+$ P14 cells (GSM3568611, GSM3568612, and GSM3568613) versus Klrg1$^-$ P14 cells (GSM3568614, GSM3568615, and GSM3568616), both at d7 after LCMV Arm infection (*47*). Genes were considered differentially expressed when [$\log_2$(fold change) > 1.5] (data file S2). A module score was calculated for each gene signature using the AddModuleScore function in the Seurat package (*62*).

ATAC-seq analysis

Purified *Tcf7*^{GFP} P14 cells (CD45.2) were adoptively transferred into B6 mice (CD45.1) before infection with LCMV Arm. At d4 and d8 p.i., *Tcf7*$^{GFP+}$, *Tcf7*$^{GFP-}$ Klrg1$^-$, and *Tcf7*$^{GFP-}$ Klrg1$^+$ P14 cells were sorted from the spleens of infected recipient mice or from naïve *Tcf7*^{GFP} P14 mice, and three replicates (5×10^4 cells) of each population were subjected to bulk ATAC-seq analysis as described in Supplementary Methods. ATAC-seq peaks were associated to the gene that was closest and located within <5 kb of the gene body. We further incorporated our prior chromatin accessibility data from d28 *Tcf7*$^+$ (T_{CM}) and d28 *Tcf7*$^-$ samples (T_{EM}) (three replicates each) into the analyses (*22*). The reads overlapping peaks were counted with the dba.count function, followed by normalization and differential accessibility analysis as described above. We transformed the sequencing counts to $\log_2$(counts per million + 1) using the cpm function of edgeR (v3.34.1) (*63*) and calculated for each sample the average chromatin accessibility of all peaks associated with a gene.

Data normalization

The number of P14 cells per spleen (output) was recalculated as if 10^4 cells had been transferred. In addition, for all time points, we took into account that the effective take of the transferred cells was 10% (*64*). Output counts were thus normalized to an effective input of 10^4 cells. The fold expansion of P14 cells was also estimated relative to an estimated 10% "take" of the adoptively transferred naïve P14 cells (*64*).

Statistical analyses

Statistical analyses were performed using Prism 8.0 or 9.0 (Graphpad Software). Nonpaired Student's *t* test (two-tailed, 95% confidence level) was used for the comparison of two datasets. Analysis of variance (ANOVA) was used for >2 comparison groups. *P* values were considered significant when $P < 0.05$, indicated as (*$P < 0.05$, **$P < 0.01$, ***$P < 0.001$, ****$P < 0.0001$); $P > 0.05$ was considered nonsignificant (ns).

Supplementary Materials

This PDF file includes:
Supplementary Methods
Figs. S1 to S11
References (*65–75*)

Other Supplementary Material for this manuscript includes the following:
Data files S1 to S5
MDAR Reproducibility Checklist

REFERENCES AND NOTES

1. P. Graef, V. R. Buchholz, C. Stemberger, M. Flossdorf, L. Henkel, M. Schiemann, I. Drexler, T. Höfer, S. R. Riddell, D. H. Busch, Serial transfer of single-cell-derived immunocompetence reveals stemness of CD8$^+$ central memory T cells. *Immunity* **41**, 116–126 (2014).
2. A. Lanzavecchia, F. Sallusto, Progressive differentiation and selection of the fittest in the immune response. *Nat. Rev. Immunol.* **2**, 982–987 (2002).
3. S. M. Kaech, W. Cui, Transcriptional control of effector and memory CD8$^+$ T cell differentiation. *Nat. Rev. Immunol.* **12**, 749–761 (2012).
4. A. N. Henning, R. Roychoudhuri, N. P. Restifo, Epigenetic control of CD8$^+$ T cell differentiation. *Nat. Rev. Immunol.* **18**, 340–356 (2018).
5. V. R. Buchholz, T. N. M. Schumacher, D. H. Busch, T cell fate at the single-cell level. *Annu. Rev. Immunol.* **34**, 65–92 (2016).
6. O. Bannard, M. Kraman, D. T. Fearon, Secondary replicative function of CD8$^+$ T cells that had developed an effector phenotype. *Science* **323**, 505–509 (2009).
7. B. Youngblood, J. S. Hale, H. T. Kissick, E. Ahn, X. Xu, A. Wieland, K. Araki, E. E. West, H. E. Ghoneim, Y. Fan, P. Dogra, C. W. Davis, B. T. Konieczny, R. Antia, X. Cheng, R. Ahmed, Effector CD8 T cells dedifferentiate into long-lived memory cells. *Nature* **552**, 404–409 (2017).
8. N. S. Joshi, W. Cui, A. Chandele, H. K. Lee, D. R. Urso, J. Hagman, L. Gapin, S. M. Kaech, Inflammation directs memory precursor and short-lived effector CD8$^+$ T cell fates via the graded expression of T-bet transcription factor. *Immunity* **27**, 281–295 (2007).
9. J. T. Chang, V. R. Palanivel, I. Kinjyo, F. Schambach, A. M. Intlekofer, A. Banerjee, S. A. Longworth, K. E. Vinup, P. Mrass, J. Oliaro, N. Killeen, J. S. Orange, S. M. Russell, W. Weninger, S. L. Reiner, Asymmetric T lymphocyte division in the initiation of adaptive immune responses. *Science* **315**, 1687–1691 (2007).
10. B. Kakaradov, J. Arsenio, C. E. Widjaja, Z. He, S. Aigner, P. J. Metz, B. Yu, E. J. Wehrens, J. Lopez, S. H. Kim, E. I. Zuniga, A. W. Goldrath, J. T. Chang, G. W. Yeo, Early transcriptional and epigenetic regulation of CD8$^+$ T cell differentiation revealed by single-cell RNA sequencing. *Nat. Immunol.* **18**, 422–432 (2017).
11. N. P. Restifo, L. Gattinoni, Lineage relationship of effector and memory T cells. *Curr. Opin. Immunol.* **25**, 556–563 (2013).
12. V. Kalia, S. Sarkar, S. Subramaniam, W. N. Haining, K. A. Smith, R. Ahmed, Prolonged interleukin-2Ralpha expression on virus-specific CD8$^+$ T cells favors terminal-effector differentiation in vivo. *Immunity* **32**, 91–103 (2010).
13. V. P. Badovinac, K. A. N. Messingham, A. Jabbari, J. S. Haring, J. T. Harty, Accelerated CD8$^+$ T-cell memory and prime-boost response after dendritic-cell vaccination. *Nat. Med.* **11**, 748–756 (2005).
14. G. R. Starbeck-Miller, H. H. Xue, J. T. Harty, IL-12 and type I interferon prolong the division of activated CD8 T cells by maintaining high-affinity IL-2 signaling in vivo. *J. Exp. Med.* **211**, 105–120 (2014).
15. B. H. Ladle, K. P. Li, M. J. Phillips, A. B. Pucsek, A. Haile, J. D. Powell, E. M. Jaffee, D. A. Hildeman, C. J. Gamper, De novo DNA methylation by DNA methyltransferase 3a controls early effector CD8$^+$ T-cell fate decisions following activation. *Proc. Natl. Acad. Sci. U.S.A.* **113**, 10631–10636 (2016).

16. S. M. Gray, R. A. Amezquita, T. Guan, S. H. Kleinstein, S. M. Kaech, Polycomb repressive complex 2-mediated chromatin repression guides effector CD8$^+$ T cell terminal differentiation and loss of multipotency. *Immunity* **46**, 596–608 (2017).
17. L. Pace, C. Goudot, E. Zueva, P. Gueguen, N. Burgdorf, J. J. Waterfall, J. P. Quivy, G. Almouzni, S. Amigorena, The epigenetic control of stemness in CD8$^+$ T cell fate commitment. *Science* **359**, 177–186 (2018).
18. X. Zhou, S. Yu, D.-M. Zhao, J. T. Harty, V. P. Badovinac, H.-H. Xue, Differentiation and persistence of memory CD8$^+$ T cells depend on T cell factor 1. *Immunity* **33**, 229–240 (2010).
19. G. Jeannet, C. Boudousquié, N. Gardiol, J. Kang, J. Huelsken, W. Held, Essential role of the Wnt pathway effector Tcf-1 for the establishment of functional CD8 T cell memory. *Proc. Natl. Acad. Sci. U.S.A.* **107**, 9777–9782 (2010).
20. M. Danilo, V. Chennupati, J. Gomes Silva, S. Siegert, W. Held, Suppression of Tcf1 by inflammatory cytokines facilitates effector CD8 T cell differentiation. *Cell Rep.* **22**, 2107–2117 (2018).
21. W.-H. W. Lin, S. A. Nish, B. Yen, Y.-H. Chen, W. C. Adams, R. Kratchmarov, N. J. Rothman, A. Bhandoola, H.-H. Xue, S. L. Reiner, CD8$^+$ T lymphocyte self-renewal during effector cell determination. *Cell Rep.* **17**, 1773–1782 (2016).
22. D. Pais Ferreira, J. G. Silva, T. Wyss, S. A. Fuertes Marraco, L. Scarpellino, M. Charmoy, R. Maas, I. Siddiqui, L. Tang, J. A. Joyce, M. Delorenzi, S. A. Luther, D. E. Speiser, W. Held, Central memory CD8$^+$ T cells derive from stem-like *Tcf7*^{hi} effector cells in the absence of cytotoxic differentiation. *Immunity* **53**, 985–1000.e11 (2020).
23. J. J. Obar, L. Lefrancois, Early signals during CD8 T cell priming regulate the generation of central memory cells. *J. Immunol.* **185**, 263–272 (2010).
24. V. R. Buchholz, M. Flossdorf, I. Hensel, L. Kretschmer, B. Weissbrich, P. Gräf, A. Verschoor, M. Schiemann, T. Höfer, D. H. Busch, Disparate individual fates compose robust CD8$^+$ T cell immunity. *Science* **340**, 630–635 (2013).
25. L. Kretschmer, M. Flossdorf, J. Mir, Y. L. Cho, M. Plambeck, I. Treise, A. Toska, S. Heinzel, M. Schiemann, D. H. Busch, V. R. Buchholz, Differential expansion of T central memory precursor and effector subsets is regulated by division speed. *Nat. Commun.* **11**, 113 (2020).
26. J. B. Johnnidis, Y. Muroyama, S. F. Ngiow, Z. Chen, S. Manne, Z. Cai, S. Song, J. M. Platt, J. M. Schenkel, M. Abdel-Hakeem, J.-C. Beltra, A. R. Greenplate, M.-A. A. Ali, K. Nzingha, J. R. Giles, C. Harly, J. Attanasio, K. E. Pauken, B. Bengsch, M. A. Paley, V. T. Tomov, M. Kurachi, D. A. A. Vignali, A. H. Sharpe, S. L. Reiner, A. Bhandoola, F. B. Johnson, E. J. Wherry, Inhibitory signaling sustains a distinct early memory CD8$^+$ T cell precursor that is resistant to DNA damage. *Sci. Immunol.* **6**, eabe3702 (2021).
27. J. R. Giles, S. F. Ngiow, S. Manne, A. E. Baxter, O. Khan, P. Wang, R. Staupe, M. S. Abdel-Hakeem, H. Huang, D. Mathew, M. M. Painter, J. E. Wu, Y. J. Huang, R. R. Goel, P. K. Yan, G. C. Karakousis, X. Xu, T. C. Mitchell, A. C. Huang, E. J. Wherry, Shared and distinct biological circuits in effector, memory and exhausted CD8$^+$ T cells revealed by temporal single-cell transcriptomics and epigenetics. *Nat. Immunol.* **23**, 1600–1613 (2022).
28. D. T. Utzschneider, M. Charmoy, V. Chennupati, L. Pousse, D. P. Ferreira, S. Calderon-Copete, M. Danilo, F. Alfei, M. Hofmann, D. Wieland, S. Pradervand, R. Thimme, D. Zehn, W. Held, T cell factor 1-expressing memory-like CD8$^+$ T cells sustain the immune response to chronic viral infections. *Immunity* **45**, 415–427 (2016).
29. N. Sevilla, S. Kunz, A. Holz, H. Lewicki, D. Homann, H. Yamada, K. P. Campbell, J. C. de la Torre, M. B. A. Oldstone, Immunosuppression and resultant viral persistence by specific viral targeting of dendritic cells. *J. Exp. Med.* **192**, 1249–1260 (2000).
30. K. Bresser, L. Kok, A. C. Swain, L. A. King, L. Jacobs, T. S. Weber, L. Perié, K. R. Duffy, R. J. de Boer, F. A. Scheeren, T. N. Schumacher, Replicative history marks transcriptional and functional disparity in the CD8$^+$ T cell memory pool. *Nat. Immunol.* **23**, 791–801 (2022).
31. I. Siddiqui, K. Schaeuble, V. Chennupati, S. A. Fuertes Marraco, S. Calderon-Copete, D. Pais Ferreira, S. J. Carmona, L. Scarpellino, D. Gfeller, S. Pradervand, S. A. Luther, D. E. Speiser, W. Held, Intratumoral Tcf1$^+$PD-1$^+$CD8$^+$ T cells with stem-like properties promote tumor control in response to vaccination and checkpoint blockade immunotherapy. *Immunity* **50**, 195–211.e10 (2019).
32. A. F. Christiaansen, P. M. Boggiatto, S. M. Varga, Limitations of Foxp3$^+$ Treg depletion following viral infection in DEREG mice. *J. Immunol. Methods* **406**, 58–65 (2014).
33. C. F. Schaefer, K. Anthony, S. Krupa, J. Buchoff, M. Day, T. Hannay, K. H. Buetow, PID: The Pathway Interaction Database. *Nucleic Acids Res.* **37**, D674–D679 (2009).
34. A. Liberzon, C. Birger, H. Thorvaldsdóttir, M. Ghandi, J. P. Mesirov, P. Tamayo, The Molecular Signatures Database (MSigDB) hallmark gene set collection. *Cell Syst.* **1**, 417–425 (2015).
35. T. A. E. Elliot, E. K. Jennings, D. A. J. Lecky, N. Thawait, A. Flores-Langarica, A. Copland, K. M. Maslowski, D. C. Wraith, D. Bending, Antigen and checkpoint receptor engagement recalibrates T cell receptor signal strength. *Immunity* **54**, 2481–2496.e6 (2021).
36. D. Zehn, S. Y. Lee, M. J. Bevan, Complete but curtailed T-cell response to very low-affinity antigen. *Nature* **458**, 211–214 (2009).
37. A. C. Richard, A. T. L. Lun, W. W. Y. Lau, B. Göttgens, J. C. Marioni, G. M. Griffiths, T cell cytolytic capacity is independent of initial stimulation strength. *Nat. Immunol.* **19**, 849–858 (2018).
38. S. Johnson, A. Bergthaler, F. Graw, L. Flatz, W. V. Bonilla, C.-A. Siegrist, P.-H. Lambert, R. R. Regoes, D. D. Pinschewer, Protective efficacy of individual CD8$^+$ T cell specificities in chronic viral infection. *J. Immunol.* **194**, 1755–1762 (2015).
39. D. T. Utzschneider, F. Alfei, P. Roelli, D. Barras, V. Chennupati, S. Darbre, M. Delorenzi, D. D. Pinschewer, D. Zehn, High antigen levels induce an exhausted phenotype in a chronic infection without impairing T cell expansion and survival. *J. Exp. Med.* **213**, 1819–1834 (2016).
40. M. E. Pipkin, J. A. Sacks, F. Cruz-Guilloty, M. G. Lichtenheld, M. J. Bevan, A. Rao, Interleukin-2 and inflammation induce distinct transcriptional programs that promote the differentiation of effector cytolytic T cells. *Immunity* **32**, 79–90 (2010).
41. S. J. Keppler, K. Rosenits, T. Koegl, S. Vucikuja, P. Aichele, Signal 3 cytokines as modulators of primary immune responses during infections: The interplay of type I IFN and IL-12 in CD8 T cell responses. *PLOS ONE* **7**, e40865 (2012).
42. J. Crouse, G. Bedenikovic, M. Wiesel, M. Ibberson, I. Xenarios, D. von Laer, U. Kalinke, E. Vivier, S. Jonjic, A. Oxenius, Type I interferons protect T cells against NK cell attack mediated by the activating receptor NCR1. *Immunity* **40**, 961–973 (2014).
43. J. R. Teijaro, C. Ng, A. M. Lee, B. M. Sullivan, K. C. F. Sheehan, M. Welch, R. D. Schreiber, J. Carlos de la Torre, M. B. A. Oldstone, Persistent LCMV infection is controlled by blockade of type I interferon signaling. *Science* **340**, 207–211 (2013).
44. E. J. Wherry, S.-J. Ha, S. M. Kaech, W. N. Haining, S. Sarkar, V. Kalia, S. Subramaniam, J. N. Blattman, D. L. Barber, R. Ahmed, Molecular signature of CD8$^+$ T cell exhaustion during chronic viral infection. *Immunity* **27**, 670–684 (2007).
45. W. Cui, N. S. Joshi, A. Jiang, S. M. Kaech, Effects of signal 3 during CD8 T cell priming: Bystander production of IL-12 enhances effector T cell expansion but promotes terminal differentiation. *Vaccine* **27**, 2177–2187 (2009).
46. N. Palacio, T. Dangi, Y. R. Chung, Y. Wang, J. L. Loredo-Varela, Z. Zhang, P. Penaloza-MacMaster, Early type I IFN blockade improves the efficacy of viral vaccines. *J. Exp. Med.* **217**, e20191220 (2020).
47. C. Yao, H. W. Sun, N. E. Lacey, Y. Ji, E. A. Moseman, H. Y. Shih, E. F. Heuston, M. Kirby, S. Anderson, J. Cheng, O. Khan, R. Handon, J. Reilley, J. Fioravanti, J. Hu, S. Gossa, E. J. Wherry, L. Gattinoni, D. B. McGavern, J. J. O'Shea, P. L. Schwartzberg, T. Wu, Single-cell RNA-seq reveals TOX as a key regulator of CD8$^+$ T cell persistence in chronic infection. *Nat. Immunol.* **20**, 890–901 (2019).
48. P.-O. Esteve, U. S. Vishnu, H. G. Chin, S. Pradhan, Visualization and sequencing of accessible chromatin reveals cell cycle and post-HDAC inhibitor treatment dynamics. *J. Mol. Biol.* **432**, 5304–5321 (2020).
49. S. M. Kaech, R. Ahmed, Memory CD8$^+$ T cell differentiation: Initial antigen encounter triggers a developmental program in naïve cells. *Nat. Immunol.* **2**, 415–422 (2001).
50. M. J. B. van Stipdonk, E. E. Lemmens, S. P. Schoenberger, Naïve CTLs require a single brief period of antigenic stimulation for clonal expansion and differentiation. *Nat. Immunol.* **2**, 423–429 (2001).
51. S. Sarkar, V. Kalia, W. N. Haining, B. T. Konieczny, S. Subramaniam, R. Ahmed, Functional and genomic profiling of effector CD8 T cell subsets with distinct memory fates. *J. Exp. Med.* **205**, 625–640 (2008).
52. J. P. Scott-Browne, I. F. López-Moyado, S. Trifari, V. Wong, L. Chavez, A. Rao, R. M. Pereira, Dynamic changes in chromatin accessibility occur in CD8$^+$ T cells responding to viral infection. *Immunity* **45**, 1327–1340 (2016).
53. D. Wang, H. Diao, A. J. Getzler, W. Rogal, M. A. Frederick, J. Milner, B. Yu, S. Crotty, A. W. Goldrath, M. E. Pipkin, The transcription factor Runx3 establishes chromatin accessibility of cis-regulatory landscapes that drive memory cytotoxic T lymphocyte formation. *Immunity* **48**, 659–674.e6 (2018).
54. R. R. Jadhav, S. J. Im, B. Hu, M. Hashimoto, P. Li, J.-X. Lin, W. J. Leonard, W. J. Greenleaf, R. Ahmed, J. J. Goronzy, Epigenetic signature of PD-1$^+$ TCF1$^+$ CD8 T cells that act as resource cells during chronic viral infection and respond to PD-1 blockade. *Proc. Natl. Acad. Sci. U.S.A.* **116**, 14113–14118 (2019).
55. E. Ahn, K. Araki, M. Hashimoto, W. Li, J. L. Riley, J. Cheung, A. H. Sharpe, G. J. Freeman, B. A. Irving, R. Ahmed, Role of PD-1 during effector CD8 T cell differentiation. *Proc. Natl. Acad. Sci. U.S.A.* **115**, 4749–4754 (2018).
56. M. J. B. van Stipdonk, G. Hardenberg, M. S. Bijker, E. E. Lemmens, N. M. Droin, D. R. Green, S. P. Schoenberger, Dynamic programming of CD8$^+$ T lymphocyte responses. *Nat. Immunol.* **4**, 361–365 (2003).
57. H. Pircher, T. W. Mak, R. Lang, W. Ballhausen, E. Rüedi, H. Hengartner, R. M. Zinkernagel, K. Bürki, T cell tolerance to Mlsa encoded antigens in T cell receptor V beta 8.1 chain transgenic mice. *EMBO J.* **8**, 719–727 (1989).

58. S. Verbeek, D. Izon, F. Hofhuis, E. Robanus-Maandag, H. te Riele, M. van de Wetering, M. Oosterwegel, A. Wilson, H. Robson MacDonald, H. Clevers, An HMG-box-containing T-cell factor required for thymocyte differentiation. *Nature* **374**, 70–74 (1995).
59. H. J. Snippert, L. G. van der Flier, T. Sato, J. H. van Es, M. van den Born, C. Kroon-Veenboer, N. Barker, A. M. Klein, J. van Rheenen, B. D. Simons, H. Clevers, Intestinal crypt homeostasis results from neutral competition between symmetrically dividing Lgr5 stem cells. *Cell* **143**, 134–144 (2010).
60. L. Madisen, T. A. Zwingman, S. M. Sunkin, S. W. Oh, H. A. Zariwala, H. Gu, L. L. Ng, R. D. Palmiter, M. J. Hawrylycz, A. R. Jones, E. S. Lein, H. Zeng, A robust and high-throughput Cre reporting and characterization system for the whole mouse brain. *Nat. Neurosci.* **13**, 133–140 (2010).
61. T. Wu, E. Hu, S. Xu, M. Chen, P. Guo, Z. Dai, T. Feng, L. Zhou, W. Tang, L. Zhan, X. Fu, S. Liu, X. Bo, G. Yu, ClusterProfiler 4.0: A universal enrichment tool for interpreting omics data. *Innovation* **2**, 100141 (2021).
62. I. Tirosh, B. Izar, S. M. Prakadan, M. H. Wadsworth II, D. Treacy, J. J. Trombetta, A. Rotem, C. Rodman, C. Lian, G. Murphy, M. Fallahi-Sichani, K. Dutton-Regester, J. R. Lin, O. Cohen, P. Shah, D. Lu, A. S. Genshaft, T. K. Hughes, C. G. K. Ziegler, S. W. Kazer, A. Gaillard, K. E. Kolb, A. C. Villani, C. M. Johannessen, A. Y. Andreev, E. M. van Allen, M. Bertagnolli, P. K. Sorger, R. J. Sullivan, K. T. Flaherty, D. T. Frederick, J. Jané-Valbuena, C. H. Yoon, O. Rozenblatt-Rosen, A. K. Shalek, A. Regev, L. A. Garraway, Dissecting the multicellular ecosystem of metastatic melanoma by single-cell RNA-seq. *Science* **352**, 189–196 (2016).
63. M. D. Robinson, D. J. McCarthy, G. K. Smyth, EdgeR: A Bioconductor package for differential expression analysis of digital gene expression data. *Bioinformatics* **26**, 139–140 (2010).
64. J. N. Blattman, R. Antia, D. J. D. Sourdive, X. Wang, S. M. Kaech, K. Murali-Krishna, J. D. Altman, R. Ahmed, Estimating the precursor frequency of naive antigen-specific CD8 T cells. *J. Exp. Med.* **195**, 657–664 (2002).
65. Y. Hao, S. Hao, E. Andersen-Nissen, W. M. Mauck III, S. Zheng, A. Butler, M. J. Lee, A. J. Wilk, C. Darby, M. Zager, P. Hoffman, M. Stoeckius, E. Papalexi, E. P. Mimitou, J. Jain, A. Srivastava, T. Stuart, L. M. Fleming, B. Yeung, A. J. Rogers, J. M. McElrath, C. A. Blish, R. Gottardo, P. Smibert, R. Satija, Integrated analysis of multimodal single-cell data. *Cell* **184**, 3573–3587.e29 (2021).
66. M. E. Ritchie, B. Phipson, D. Wu, Y. Hu, C. W. Law, W. Shi, G. K. Smyth, limma powers differential expression analyses for RNA-sequencing and microarray studies. *Nucleic Acids Res.* **43**, e47 (2015).
67. C. W. Law, Y. Chen, W. Shi, G. K. Smyth, Voom: Precision weights unlock linear model analysis tools for RNA-seq read counts. *Genome Biol.* **15**, R29 (2014).
68. B. Phipson, S. Lee, I. J. Majewski, W. S. Alexander, G. K. Smyth, Robust hyperparameter estimation protects against hypervariable genes and improves power to detect differential expression. *Ann. Appl. Stat.* **10**, 946–963 (2016).
69. Y. Benjamini, Y. Hochberg, Controlling the false discovery rate: A practical and powerful approach to multiple testing. *J. R Stat. Soc. B* **57**, 289–300 (1995).
70. J. D. Buenrostro, B. Wu, H. Y. Chang, W. J. Greenleaf, ATAC-seq: A method for assaying chromatin accessibility genome-wide. *Curr. Protoc. Mol. Biol.* **109**, 21. 29. 1–21. 29. 9 (2015).
71. J. P. Didion, M. Martin, F. S. Collins, Atropos: Specific, sensitive, and speedy trimming of sequencing reads. *PeerJ* **5**, e3720 (2017).
72. H. Li, B. Handsaker, A. Wysoker, T. Fennell, J. Ruan, N. Homer, G. Marth, G. Abecasis, R. Durbin; 1000 Genome Project Data Processing Subgroup, The Sequence Alignment/Map format and SAMtools. *Bioinformatics* **25**, 2078–2079 (2009).
73. F. Ramirez, D. P. Ryan, B. Grüning, V. Bhardwaj, F. Kilpert, A. S. Richter, S. Heyne, F. Dündar, T. Manke, DeepTools2: A next generation web server for deep-sequencing data analysis. *Nucleic Acids Res.* **44**, W160–W165 (2016).
74. A. Tarasov, A. J. Vilella, E. Cuppen, I. J. Nijman, P. Prins, Sambamba: Fast processing of NGS alignment formats. *Bioinformatics* **31**, 2032–2034 (2015).
75. Y. Zhang, T. Liu, C. A. Meyer, J. Eeckhoute, D. S. Johnson, B. E. Bernstein, C. Nusbaum, R. M. Myers, M. Brown, W. Li, X. S. Liu, Model-based analysis of ChIP-Seq (MACS). *Genome Biol.* **9**, R137 (2008).
76. S. Heinz, C. Benner, N. Spann, E. Bertolino, Y. C. Lin, P. Laslo, J. X. Cheng, C. Murre, H. Singh, C. K. Glass, Simple combinations of lineage-determining transcription factors prime cis-regulatory elements required for macrophage and B cell identities. *Mol. Cell* **38**, 576–589 (2010).

Acknowledgments: We are grateful to D. Speiser and A. Pelletier for critical reading of the manuscript, to C. Fumey for mouse management, the UNIL Flow Cytometry Facility for expert assistance with flow cytometry, and the UNIL Genomic Technologies Facility for sequencing analyses. **Funding:** This work was supported in part by funding provided by the Swiss National Science Foundation (SNSF) (310030B_179570 and 310030_200898) and the Swiss Cancer Research Foundation (KFS-3601-02-2015 and KFS-5386-08-2021) to W.H. **Author contributions:** J.G.S., D.P.F., A.D., and W.H. conceived the study. J.G.S., D.P.F., A.D., T.W., R.V., M.D., M.C. designed and performed experiments as well as analyzed and interpreted the data. D.D.P. contributed valuable virus strains. W.H. acquired funding and supervised the study. D.P.F., A.D., D.D.P., and W.H. wrote the original draft. A.D., R.V., M.C., and W.H. revised and edited the manuscript. **Competing interests:** D.D.P. is a founder, consultant, and shareholder of Hookipa Pharma Inc., commercializing arenavirus-based vector technology, and is listed as inventor on corresponding patents. The other authors declare that they have no competing interests. **Data and materials availability:** *Tcf7*^{GFP}, *Tcf7*$^{DTR\text{-}GFP}$, and *Tcf7*$^{GFP\text{-}iCre}$ mice are available from W.H. under a material transfer agreement with the University of Lausanne. RNA-seq and ATAC-seq datasets generated in this study are deposited to the Gene Expression Omnibus database under accession number GEO: GSE221969. All data needed to evaluate the conclusions in the paper are present in the paper or the Supplementary Materials.

Submitted 23 February 2023
Accepted 23 October 2023
Published 17 November 2023
10.1126/sciimmunol.adh3113

Science Immunology

Emergence and fate of stem cell–like *Tcf7*+ CD8+ T cells during a primary immune response to viral infection

Joana Gomes Silva, Daniela Pais Ferreira, Alexandre Dumez, Tania Wyss, Romain Veber, Maxime Danilo, Daniel D. Pinschewer, Mélanie Charmoy, and Werner Held

Sci. Immunol. **8** (89), eadh3113. DOI: 10.1126/sciimmunol.adh3113